

**TACTILE FEEDBACK OF STEER-BY-WIRE  
AGRICULTURE MACHINES**

by  
Hong Xu

A thesis submitted to the Faculty of the University of Delaware in partial fulfillment of the requirements for the degree of Master of Science in Mechanical Engineering

Fall 2009

© 2009 Hong Xu  
All Rights Reserved

**TACTILE FEEDBACK OF STEER-BY-WIRE  
AGRICULTURE MACHINES**

by

Hong Xu

Approved: \_\_\_\_\_  
Jian-Qiao Sun, Ph.D.  
Professor in charge of thesis on behalf of the Advisory Committee

Approved: \_\_\_\_\_  
Anette M.Karlsson, Ph.D.  
Chair of the Department of Mechanical Engineering

Approved: \_\_\_\_\_  
Michael Chajes, Ph.D.  
Dean of the College of Engineering

Approved: \_\_\_\_\_  
Debra Hess Norris, M.S.  
Vice Provost for Graduate and Professional Education

## ACKNOWLEDGEMENTS

I would like to express my gratitude to Dr. J. Q. Sun for his guidance during my studies at the University of Delaware. I thank him for his time, patience and guidance of my work, especially his support after he left for the University of California. I would also like to thank my master committee members Dr. Deng and Dr. Sarkar for taking their time to evaluate my thesis and for their feedback.

I would like to thank Chris Foster and Rick Strosser in CNH American LLC (Case-New Holland) for their support of my work. Especially, I would like to thank Chris for giving me the opportunity and guidance to do some real work in CNH company.

I would also like to take this opportunity to thank my lab mates Andrew Davison, Joseph White, Spencer Popejoy, Huseyin Denli and Bo Song for the warm environment and friendship in the Applied Controls Lab. I am grateful for them to share their experience in doing research.

Finally, I thank my parents and sister in China. They have always been supportive during my education. I appreciate the constant encouragement from my husband Zhongmin. I am grateful for his accompany and building my confidence during my whole study.

# TABLE OF CONTENTS

<b>LIST OF FIGURES</b> . . . . .	<b>vi</b>
<b>LIST OF TABLES</b> . . . . .	<b>x</b>
<b>ABSTRACT</b> . . . . .	<b>xi</b>

## Chapter

<b>1 INTRODUCTION</b> . . . . .	<b>1</b>
<b>2 SYSTEM HARDWARE DESCRIPTION</b> . . . . .	<b>6</b>
2.1 Tactile Feedback of Steer-by-Wire Agricultural Machines . . . . .	6
2.2 Introduction of Steer-By-Wire Vehicle Prototype . . . . .	6
2.3 Ground Drive Hardware . . . . .	9
2.3.1 Electronic Displacement Control Pumps and Hydraulic Motors . . . . .	9
2.3.2 Differential Steering . . . . .	10
2.3.3 Steer-by-Wire Controller . . . . .	12
2.4 Tactile Feedback Device Hardware . . . . .	14
2.4.1 Direct Current Electric Geared Motor . . . . .	14
2.4.2 Quadrature Encoder . . . . .	15
2.4.3 Steering Column Modifications . . . . .	16
2.4.4 Pressure Transducers . . . . .	17
2.5 Tactile Feedback Device Electronic Controller . . . . .	21
2.5.1 Input Circuits . . . . .	21
2.5.2 H-bridge to Drive DC Motor . . . . .	22

<b>3</b>	<b>SYSTEM MODELING</b>	<b>24</b>
3.1	Introduction	24
3.2	Theoretical Model of the Steering Control System	25
3.3	Motivation for System Identification	26
3.4	A Review of Digital Filters	27
3.4.1	System Parameter Identification Using FIR Filter	28
3.4.2	System Parameter Identification Using IIR Filter	30
3.5	Data Acquisition	32
3.6	Data Analysis and Model Selection	35
3.7	System Modeling	38
3.7.1	Model Selection	38
3.7.2	Convergence of the Mean Weight Vector	44
3.7.3	Transfer Function of the System	46
<b>4</b>	<b>TACTILE FEEDBACK CONTROL</b>	<b>48</b>
4.1	Introduction	48
4.2	Control Architecture	48
4.3	Current Control	49
4.3.1	Current Control Algorithm Design	52
4.4	Switching Control	54
4.5	Stability Analysis	57
4.6	Simulations	64
<b>5</b>	<b>SUMMARY</b>	<b>71</b>
	<b>BIBLIOGRAPHY</b>	<b>73</b>

## LIST OF FIGURES

<b>2.1</b>	A New Holland HW365 self-propelled windrower with a 2355 header cutting forage. The rows of crop the vehicle creates are called ‘windrows’, hence the name windrower. Image courtesy of CNH America LLC. . . . .	8
<b>2.2</b>	Picture of an axial piston pump which powers the hydrostatic loop of a self-propelled windrower. . . . .	11
<b>2.3</b>	Picture of an axial piston motor which is powered by an axial piston pump and drives self-propelled vehicle. . . . .	11
<b>2.4</b>	Picture of vehicle main control module which is onboard the New Holland H series and CaseIH WDX series self-propelled windrowers. . . . .	12
<b>2.5</b>	Schematic diagram of the propulsion control hardware of steer-by-wire vehicles. Thick lines represent hydraulic connections and thin lines represent electrical connections. Mechanical components are represented graphically. . . . .	13
<b>2.6</b>	An illustration of modified steering system which DC motor and quadrature encoder installed on the steering column for the purpose of tactile feedback control. . . . .	14
<b>2.7</b>	A modified steering column has been mounted to the cab of the prototype windrower. . . . .	18
<b>2.8</b>	A picture taken from underneath and front of the cab to show how the steering column attaches to the cab of the windrower through the hole on the cab floor. . . . .	19
<b>2.9</b>	An illustration of H bridge which is used to achieve both clockwise and counter-clockwise spin of DC motor in the control process. . . . .	22

<b>3.1</b>	Block diagram of adaptive filter used for system identification. . . . .	25
<b>3.2</b>	Diagram of equivalent electric circuit of a DC motor. . . . .	26
<b>3.3</b>	The electric circuit diagram for data acquisition of steering column system identification experiment. . . . .	33
<b>3.4</b>	A simplified version of the electric circuit for data acquisition of steering column system identification experiment. . . . .	34
<b>3.5</b>	A picture of the testbed for data acquisition of steering column system identification experiment. . . . .	35
<b>3.6</b>	Voltage duty cycle applied to the steering column system. This reflects the real voltage input to the system. . . . .	36
<b>3.7</b>	Pulse count of encoder channel A in every 10 miliseconds. . . . .	37
<b>3.8</b>	Spectrum of steer-by-wire system input voltage. . . . .	39
<b>3.9</b>	Spectrum of steer-by-wire system output angular velocity. . . . .	40
<b>3.10</b>	A Bode plot of steer-by-wire system transfer function. . . . .	41
<b>3.11</b>	This is a root mean squares plot of all fitted FIR and IIR models of order 4 and less. It is shown there is no big difference between FIR and IIR filters if the order is 2 or higher. . . . .	43
<b>3.12</b>	The output signals of the second order IIR adaptive filter and the steering column system are coincident except at the inflections. . . . .	44
<b>3.13</b>	This diagram shows that the difference between the output signals of the second order IIR adaptive filter and the steering column system is within 5% except at the inflexions. . . . .	45
<b>3.14</b>	The weights of the second order IIR filter converge after 1000 iterations. . . . .	47

<b>4.1</b>	This chart describes the control architecture of the whole steer-by-wire vehicle system. Tactile feedback controller is used to recover the mechanical linkage resistance. A current sense controller is used to regulate electric current of the DC motor. . . . .	49
<b>4.2</b>	Block diagram of the current control loop. . . . .	50
<b>4.3</b>	Circuit diagram of current sensing filter (a second order analogue filter). R56 is the current sensing resistor. The input comes in on CN2-A4 and the output is connected to the 10-bit analogue to digital (A/D) converter at CRSNS5. . . . .	51
<b>4.4</b>	Root locus of the current control loop. x: Open loop poles. o: Open loop zeros. $\Delta$ : Closed loop poles at $z = 0.275 \pm j0.294$ . . . . .	53
<b>4.5</b>	The switching of different controllers according to the steering wheel angle and angular velocity. . . . .	54
<b>4.6</b>	The impulse response shows that the plant is stable. . . . .	58
<b>4.7</b>	The step response of the plant shows that it is a slow system. The rise time is around 0.7 second. . . . .	59
<b>4.8</b>	Diagram of closed transfer function. . . . .	60
<b>4.9</b>	The necessary condition of Routh's stability test is that all the parameters in closed system transfer function is greater than zero. That is the control parameter $K_p$ and $K_i$ should be above all the lines in the above diagram. . . . .	62
<b>4.10</b>	Step response of the PI controller with $K_{p\_lin} = -1$ , $K_{i\_lin} = 10$ . The solid line represents the step input signal. The dash-dot line is the control signal. The dashed line is the output response. The rising time and over shoot are all big. Steady state error is zero. . .	66
<b>4.11</b>	Step response of the PI controller with $K_{p\_lin} = -1$ , $K_{i\_lin} = 50$ . The solid line represents the step input signal. The dashed line is the control signal. The dash-dot line is the output response. Rising time decreases and over shoot gets bigger. Steady state error is zero. . .	67

- 4.12** Step response of the PI controller with  $K_{p\_lin} = 10$ ,  $K_{i\_lin} = 10$ . The solid line represents the step input signal. The dashed line is the control signal. The dash-dot line is the output response. Both rising time and over shoot are decreased to a small value. Steady state error is zero. . . . . 68
- 4.13** Step response of the PI controller with  $K_{p\_lin} = 50$ ,  $K_{i\_lin} = 200$ . The solid line represents the step input signal. The dashed line is the control signal. The dash-dot line is the output response. The output signal follows the input signal perfectly. . . . . 69

## LIST OF TABLES

<b>2.1</b>	Parameters of a New Holland HW365 with 2358 disc header. This was one of the vehicles used in the experiments. . . . .	7
<b>4.1</b>	Effects of PI controller parameters on the closed-loop system response. This can be a guidance of PI tuning for Tactile feedback control system. . . . .	65
<b>4.2</b>	Control parameters used for hardware-in-loop simulation. . . . .	70

## ABSTRACT

The implementation of control systems in the automotive industry enabled by electronic actuators is referred to as X-by-wire technique. The application of steer-by-wire technique in agriculture machine simplifies manufacture, decreases machine costs and increases machine flexibility. Previous study of Applied Controls Laboratory focused on vehicle velocity control through electrical signals, which leads to drive-by-wire agriculture machines without tactile feedback. Current research focuses on the tactile feedback control of steer-by-wire vehicles where the research goal is to improve the steering maneuverability comparable to traditional mechanical steering systems. A DC motor is regulated according to the movement status of the steering wheel to produce a smooth feedback force to the operator. A prototype windrower provided by Case New Holland LLC is modulated, developed and tested for the research where a conventional steering input system is modified by being mounted with a steering input sensor and a DC geared motor. The steering input system, including the steering wheel, the steering column, the mounted sensor and the DC geared motor is mathematically modeled. The permitted angle of a steering wheel has been made up to 720 degrees in both clockwise and counter-clockwise directions whose big movement range brings a nonlinearity property into the steering mechanism. Furthermore, an H-bridge circuit has been designed and added to the control unit to enable the DC geared motor to turn in both directions. To produce the desired feedback force, two cascaded controllers have been designed. The first is a hybrid controller with multiple control branches developed to regulate the DC motor to produce the desired feedback force. Each control branch is a proportional

integral (PI) controller. The working ranges of each branch of the controller are decided according to the angle and angular velocity of the steering wheel. The stability of the designed closed loop controller is proved by Routh stability criterion and extensive simulations have been performed to verify the stability of the controller. The second is a current sense controller which is designed by the root locus method to regulate the electrical current of the DC geared motor that varies due to environmental changes. Verified by simulation, an accurate control of the feedback force can be achieved.

# Chapter 1

## INTRODUCTION

X-by-wire control systems applied in the automotive industry refer to systems where the input device manipulated by the operator is not directly connected to mechanical or hydraulic actuation power subsystems. Instead, it is connected to an embedded computer, which sends the control signals to the actuation device [8]. The “X” in the X-by-wire is replaced by “steer,” “throttle,” and “brake”, etc. to represent the steer-by-wire, throttle-by-wire, and brake-by-wire systems. Besides these, adaptive cruise control (ACC), anti-blocking system (ABS), active body control (ABC), electronic stability program (ESP), and electric power steering (EPS) are considered also as X-by-wire systems in the automotive industry. Take the brake-by-wire (BBW) system as an example. In a brake-by-wire system, a digital data bus replaces the hydraulic lines from the brake pedal to the wheel brakes. A sensor at the pedal measures the driver’s input to the controller and then the controller gives a corresponding output to drive an electric motor, which applies the required brake force to the wheel [12].

Generally, the advantages of X-by-wire systems include:

1. X-by-wire systems can simplify the assembly and lower manufacturing costs. X-by-wire vehicles will be lighter and easier to produce and maintain.
2. It is possible to make a X-by-wire system as an independent software programmable module, so it can be adapted to different vehicles without any difficulty.

3. It is the tendency that every vehicle subsystem will be replaced by X-by-wire subsystems. So it is possible to drive a vehicle by manipulating electronic signals. This provides the technology of building novel driving assistant systems for handicapped people, and even unmanned vehicles.
4. The X-by-wire systems can perform a number of functions autonomously to increase the vehicle functionality and safety. For instance, intelligent steering software can prevent an operator of a vehicle from giving a dangerous command input [8].
5. The removal of hydraulic systems can mitigate related environmental problems [11] and reduce system failure due to hydraulic system contamination dramatically.

One of the most interesting research topics among the X-by-wire domain is steer-by-wire systems applied in the automotive industry. Besides the general advantages of X-by-wire system, steer-by-wire system can improve operator performance, reduce operator fatigue and increase the productivity of the machine. Steer-by-wire system for off-road heavy vehicles contains two main subsystems. The first is the command input subsystem, which is the steering wheel. The second is the steering operating subsystem, i.e. the electrohydraulic subsystem which includes valves, cylinders, and pumps. The steering wheel and the steering control valve is connected by electrical signals, which is different from the conventional mechanical and hydraulic connections. In a conventional steering system the steering wheel rotation is proportionally amplified by the steering valve to obtain a corresponding articulation angle of the vehicle. The mechanically coupled steering mechanism will produce an inherent feedback force to the operator at the steering wheel which is proportional to the steering resistance.

The implementation of the steer-by-wire system that replaces the traditional mechanical steering system for vehicles consists of two main tasks. The first task is the maneuverability of the vehicle through electrical signals and the second is the tactile feedback control, which is designed to emulate conventional mechanical feedback to the operator. Intensive research efforts has been devoted to one or both of these two tasks by different research groups. The feasibility of steer-by-wire has been verified by both software simulations and hardware-in-loop simulations [3, 4, 10, 13–15, 17]. Some research groups have finished both the implementation of the electrical control component and the tactile feedback component of steer-by-wire passenger vehicles. [1, 2, 7, 16]. Among these implementations, either a torque sensor for the tactile feedback control is required [1] or the designed steer-by-wire system is not applicable to heavy vehicles like agriculture machines [7, 16]. The requirement of a torque sensor in the steering column not only increases the cost dramatically but also introduces an element of compliance, which affects the steering comfort and the system stability. Although permanent magnet motor has been used a lot as the actuator to drive the vehicle steering [2], due to its high power, a hydraulic system is more suitable to be the actuator to drive the steering of off-road heavy vehicles.

Few steer-by-wire subsystems for agriculture production machines are available in the market at this time. CNH America LLC has finished the study of vehicle velocity control through electrical signals in the Intelligent Control Study of Drive-by-wire Agriculture Vehicle research project [6]. Based on the previous research on the electrical control of vehicle straight forward and backward propulsion and with the concept of differential drive, we can implement the steering of a vehicle by giving different input commands to the left and right sides of the steering actuator, respectively. The main task of present work is the design of tactile feedback control of steer-by-wire agriculture machines.

The challenge of tactile feedback control of steer-by-wire vehicle is to make

sure that a suitable steering feel corresponding to the vehicle steering condition is achieved. To generate this feedback force, Rutgers University and General Motors cooperated group use two kinds of Electro-Rheological Fluids (ERF) based actuators [9]. One is the Concentric-Cylinder Actuator and the other is the Flat-Plate Actuator. Considering its cost, variability and well developed relevant theory, most researchers of this topic instead choose electrical motor to generate the feedback force [1, 4, 13, 15–17]. For the same reason an electrical motor is selected to provide the feedback force in current research.

A prototype windrower provided by Case-New Holland LLC is modulated, developed and tested for the research. The goal is to implement the steering maneuverability with desired feedback force to the operator comparable to traditional mechanical steering systems. To this goal, we modified the conventional steering input device by mounting a steering input sensor and a DC geared motor on it. The steering input system, including the steering wheel, the steering column, the mounted sensor and the DC motor is mathematically modeled. Here we use a DC motor as feedback force actuator, which gives an output torque proportional to its input current. To have an accurate control of the feedback force when there is any environmental change, such as temperature change of the motor, a current controller is designed to regulate the input signal to the DC motor.

In order to allow the steer-by-wire vehicle operator to turn the steering wheel for multiple cycles, the permitted angle of a steering wheel has been made up to 720 degrees in both clockwise and counter-clockwise directions. The big position range made it hard for a single control law to work well for the whole control process because of the nonlinear property of the steering mechanism. So a hybrid controller with multiple branches is designed, where each of the branches is actually a proportional integral (PI) controller. The control ranges of each branch are divided according to the angle and angular velocity of the steering wheel. Furthermore,

with the requirement that the actuation motor has reversible turning directions, an H-bridge circuit is integrated to the control unit.

The rest of the thesis is organized as follows: Chapter 2 gives a description of the prototype steer-by-wire windrower, its ground drive hardware and the tactile feedback device (TFD) hardware. The theory of signal processing used for steer-by-wire system identification and the steering input system modeling is discussed in Chapter 3. The tactile feedback device control algorithm design, the proof of system stability and simulations are presented in Chapter 4. This is followed by a summary of achievements in Chapter 5.

## Chapter 2

### SYSTEM HARDWARE DESCRIPTION

#### 2.1 Tactile Feedback of Steer-by-Wire Agricultural Machines

The steer-by-wire technology of agricultural machines replaces the conventional mechanical steering mechanism with an electronic actuation system. The implementation of the steer-by-wire system consists of two main tasks. The first task is the maneuverability of the vehicle through electrical control of the hydraulic systems, which involves the control of hydraulic pumps and the driving of hydraulic motors. The second is the tactile feedback control, which is to emulate conventional mechanical feedback force by regulating a DC geared motor that is mounted on the steering column. The angle and angular velocity of steering wheel are the input signals to the tactile feedback controller which are measured by a quadrature encoder. The digital control algorithms are implemented through the vehicle control modules, whose input and output circuits must be compatible for the input and output signals. Relevant hardware and characteristic of the experiment prototype vehicles are described in this chapter.

#### 2.2 Introduction of Steer-By-Wire Vehicle Prototype

A windrower is an agricultural machine used for hay and forage preparation, crop harvesting, and crop residue processing. Self-propelled windrowers are windrowers with electrical controlled propulsion system. An example of a self-propelled windrower is shown in Figure 2.1 and Table 2.1 lists some of the physical parameters of one of the vehicles used in the experiments. A self-propelled

windrower is composed of three primary sub-systems: a diesel engine to provide power, a cutting head to cut and prepare the crop and an electrical controlled ground drive system for propulsion. As a regular windrower, the primary function of a self-propelled windrower is to cut the crop and leave it in a ‘windrow’ of desired geometry. A ‘windrow’ is the row of crops that the vehicle creates after it cuts the crop which can be seen in the background of Figure 2.1. The most common use of a self-propelled windrower is in the preparation of hay or stored forage. A self-propelled windrower will cut a forage crop, ‘condition’ the crop, and leave the crop in windrows in preparation for a baler or forage harvester. They can also be used to prepare crops for combine harvesters. A combine then need not devote as much energy in cutting the crop and directing it towards the feeder house. A combine with a windrow pickup can focus its energy on the threshing and separation processes [5].

**Table 2.1:** Parameters of a New Holland HW365 with 2358 disc header. This was one of the vehicles used in the experiments.

Total vehicle mass (tractor + header)	7853 <i>kg</i>
Front wheel radius (size 23.1-26)	1493 <i>mm</i>
Wheelbase	3485 <i>mm</i>
Engine power rating	168 <i>kW</i>

The steer-by-wire vehicle prototypes used for experiments in this work are New Holland H series or CaseIH WD series self-propelled windrowers, which are provided by CNH America LLC. New Holland H series and CaseIH WD series self-propelled windrowers are fundamentally the same in regard to the work mentioned in this thesis [5]. At the beginning of the work, the prototypes were modified with steer-by-wire self-propelled windrowers of model NH H8040 and CIH WD1203, which are 4-cylinder propelled-by-wire windrowers. Because the availability of better conditioned prototype machines, the steer-by-wire configuration is transferred to NH



**Figure 2.1:** A New Holland HW365 self-propelled windrower with a 2358 header cutting forage. The rows of crop the vehicle creates are called ‘windrows’, hence the name windrower. Image courtesy of CNH America LLC.

H8060/H8080 and CIH WD1903/WD2303 windrowers both of which are 6-cylinder propelled-by-wire windrowers.

## **2.3 Ground Drive Hardware**

### **2.3.1 Electronic Displacement Control Pumps and Hydraulic Motors**

The prototype self-propelled windrowers use electric signals to control their ground propulsion. Variable displacement axial piston pumps are applied as the windrower's propulsion actuator. The primary components of an axial piston pump are cylinder block, valve plate, swash plate and a number of pistons. The pistons are arranged in a circular array within the cylinder block. One end of the cylinder block is flat and wears against a mating surface on the stationary valve plate. The pumping pistons protrude from the opposite end of the cylinder block and bear against the swash plate. The angle between a vector normal to the swash plate plane and the cylinder block axis of rotation is called swash plate angle which determines the amount of fluid pumped per shaft revolution. For a variable displacement pump whose swash plate is movable, it has the ability to vary its amount of fluid pumped per shaft revolution during operation. If the vector normal to the swash plate plane is set parallel to the axis of rotation, there is no movement of the pistons in their cylinders. Thus there is no output. Movement of the swash plate controls pump output from zero to a maximum value. So the power of the variable displacement axial piston pumps are controlled through adjusting the swash plate angle and the number of revolution per unit time.

Hydraulic motor is a mechanical actuator that converts hydraulic pressure and flow into torque and angular displacement. An axial piston motor has the same configuration as axial piston pumps. When high pressure oil flows into the chambers in the pump, the pistons protrude out and push against the swash plate. Because there is the swash plate angle, the counter force given by the swash plate can be divided into two parts. One part is parallel to the piston axis, which balances the

hydraulic force produced by the high pressure oil. The other part will produce a torque that rotates the cylinder block, thus drive the vehicle front wheels where the cylinder blocks are attached to.

### **2.3.2 Differential Steering**

The steer-by-wire prototype windrower has the property of differential steering. Differential steering of a wheeled vehicle means that each of its driving wheels is driven separately. The primary components of a steer-by-wire windrower's power train are hydrostatic loops each of which is composed of two main elements, a variable displacement hydraulic pump and a variable displacement hydraulic motor. The propulsion system consists of two independent hydrostatic loops, each driving one of the front wheels. Each hydrostatic loop is powered by a variable displacement axial piston pump, which is shown in Figure 2.5. The two hydraulic pumps for the ground drive are housed together in a tandem pump and connected to the diesel engine. Each of the pumps drives a hydraulic motor connected to a planetary hub driving one of the front wheels. As indicated in Figure 2.2, the hydraulic pumps are located in the engine compartment. As shown in Figure 2.3, the hydraulic motors are located at the hubs of the front wheels.

The speed of each wheel is proportional to the flow of oil in the corresponding hydrostatic loop. The oil flow in each loop is regulated by the rotational speed of the pumps and the adjustment of the displacement of the pumps. Rotational speed of the pumps is directly correlated to engine speed. Pump displacement is varied by changing the angle of the swash plate. The swash plate position is controlled by electronic signals. Equal flow in the two hydrostatic loops causes the front wheels to rotate at equal speeds, thus achieving a straight forward or reverse movement of the vehicle. Different flow in the two hydrostatic loops will rotate the front wheels at different speeds, making the vehicle turn either left or right.



**Figure 2.2:** Picture of an axial piston pump which powers the hydrostatic loop of a self-propelled windrower.



**Figure 2.3:** Picture of an axial piston motor which is powered by an axial piston pump and drives self-propelled vehicle.



**Figure 2.4:** Picture of vehicle main control module which is onboard the New Holland H series and CaseIH WDX series self-propelled windrowers.

A particular advantage of this type of hydrostatic transmission is the ability to perform ‘zero radius’ turns. While the vehicle is stationary the steering wheel can be turned causing one wheel to rotate in the forward direction and the other to rotate in the reverse direction. This causes the vehicle to perform a ‘zero radius’ turn, otherwise known as a ‘spin’ turn.

### **2.3.3 Steer-by-Wire Controller**

The picture of the steer-by-wire control module named XCM is shown in Figure 2.4. This is the vehicle main control module onboard the New Holland H series and CaseIH WDX series self-propelled windrowers. The main processor in the module is the Infineon C167. The controller has a variety of I/O types. The primary outputs of tactile feedback controller in this work are a set of pulse-width modulated (PWM) signals that switch between 0 and 12 V and high side driver (HSD) output ports for PWM signals are used. As shown in Figure 2.5 the input

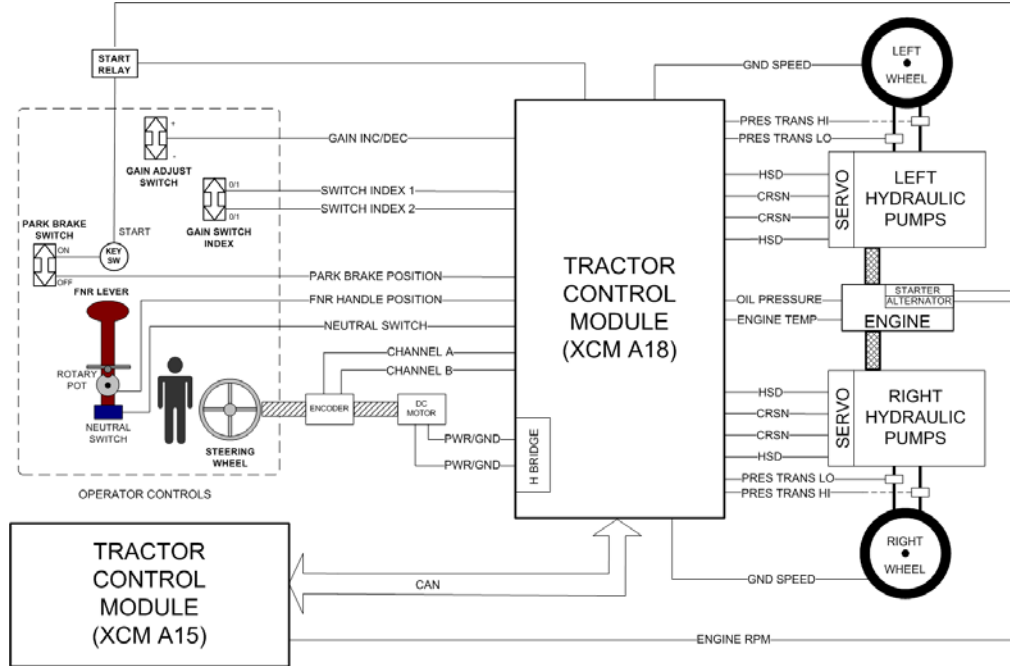


**Figure 2.5:** Schematic diagram of the propulsion control hardware of steer-by-wire vehicles. Thick lines represent hydraulic connections and thin lines represent electrical connections. Mechanical components are represented graphically.

ports of the tactile feedback controller are current sense input circuits that is for pressure transducer measurements, frequency input ports for encoder measurements, and 10-bit analog to digital (AtoD) 0-5 V channels for necessary conversions. The module is programmed in C and all calculations are performed using integer math. Consideration has to be made for overflow and resolution in real-time coding. The XCM communicates with other controllers and electronic systems on the vehicle using a controller-area-network (CAN) bus which is indicated in Figure 2.5. CAN is a serial network protocol that transfers information between ECU (Electronic Control Units) in vehicles. It is proved to be an inexpensive, robust solution for automotive control networks and is well established and used in all types of vehicles.

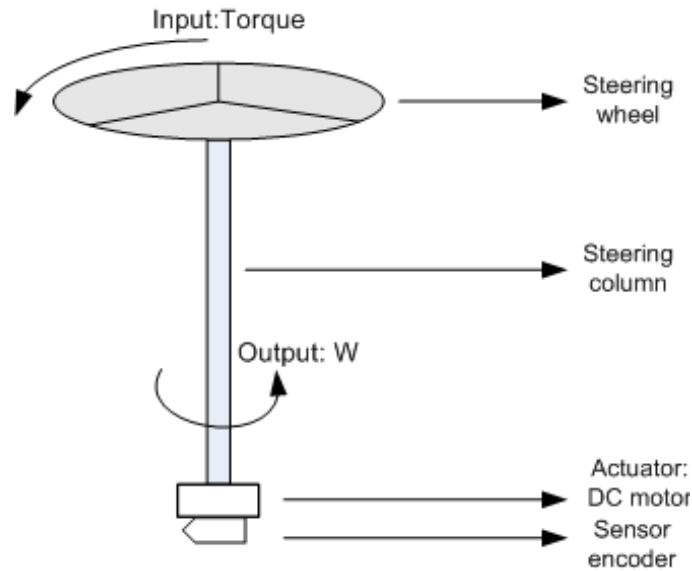


**Figure 2.6:** An illustration of modified steering system which DC motor and quadrature encoder installed on the steering column for the purpose of tactile feedback control.

## 2.4 Tactile Feedback Device Hardware

To emulate the mechanical resistance of driving conventional vehicle on drive-by-wire agriculture machines, tactile feedback device hardware have been designed by modifying conventional steering column. A DC geared motor and a quadrature encoder have been monted to the bottom of the steering column, which is shown in Figure 2.6. Pressure transducers have been used to measure the turning status of the vehicle. The hard components and tactile feedback hardware configuration are described below.

### 2.4.1 Direct Current Electric Geared Motor

A DC geared motor which is regulated by the tactile feedback controller has been attached to the steering column to provide the operator a tactile resistance during operation. The physical property of human being operation determines that

the output speed of the motor can not be high. It should be slow enough for the operator to follow comfortably and meanwhile it is important for the DC motor to provide a proper output torque. The output torque neither should be too big for the operator to handle the steering wheel, nor should be too small for the operator to feel the resistance obviously. Since a gear box can adjust the output speed and torque at the same time, a DC geared motor is ideal to be used here. When the DC geared motor is connected to the bottom of the steering column, the length of the steering column has been extended. Unfortunately there is only limited space between the bottom of the steering shaft and the cab floor when the steering column is mounted in the cab of the windrower. In addition the gear box attached to the DC motor usually takes a considerable amount of space. Thus the selection of the DC geared motor is restrained a lot. The highest electrical voltage the XCM can provide is 13.8 V, so the nominal voltage of the DC motor should be no more than 13.8 V. To meet the above requirements a 12 V DC geared motor has been selected, whose part number is CHM-1250-1M, Molon Motor and Coil Corporation. Its total length is 2.65 Inches and it needs the end of the steering column to stick into the hole in the cab floor a little bit for it to fit in the limited space. The motor produces a 10 In-lbs of output torque at its top speed of 50 RPMs and full load current of 1.2 A. The nominal resistance of the DC geared motor is 3.2155  $\Omega$ .

#### **2.4.2 Quadrature Encoder**

To make the tactile feedback controller regulating the DC geared motor to produce desired tactile feedback force, the angle and angular velocity of the steering column are measured by a quadrature encoder. A quadrature encoder is a common type of incremental encoder that use two output channels (A and B) to measure position. Using two code tracks with sectors positioned 90° out of phase, the two output channels of the quadrature encoder indicate both position and direction of rotation. If A lead B, the disk is rotating in a clockwise direction. Otherwise, the

disk is rotating in a counter-clockwise direction. Some quadrature encoders also include a third output channel, called a zero or reference signal, which produces a single pulse per revolution. This single pulse can be used for precise determination of a reference position. With their high resolutions, extreme durability and ease of installation, quadrature encoders are ideal for a wide variety of applications. The measurements from the quadrature encoder are numbers of pulses per 10 ms of the two encoder channels based on which the angle and angular velocity of the steering wheel are calculated in the controller. The calculated angle and angular velocity and the turning condition of the vehicle are the input information for the tactile feedback controller to calculate the output voltage through designed control algorithm. The controller output voltage regulates the DC geared motor so that desired pseudo tactile feedback force can be produced.

The quadrature encoder used in current research is an optical encoder from US Digital whose part number is E3-400-500-IH. E3 serial optical encoders are high resolution rotary encoders with a molded polycarbonate enclosure, which utilizes either a standard or locking 5-pin connector. This optical incremental encoder can be easily mounted to and dismount from an existing shaft to provide digital measurements. The "400" following "E3" stands for the resolution of the encoder which means it will generate 400 pulse per revolution for both channel A and channel B. "500" means the shaft diameter is 1/2 inches and "I" in the part number means the encoder has the third channel or the index channel. "H" means there is a hole in housing to allow shaft to pass through.

### **2.4.3 Steering Column Modifications**

The steering column system are not mechanically coupled to the hydraulic steering control system, but is rigidly connected to a quadratic encoder and a DC geared motor. The quadratic encoder is mounted to the steering shaft through the hole of its housing. Besides the mounting screw of the encoder is used to keep the

encoder from sliding, a bracket is also used to make sure the encoder be fixed to the place. The DC geared motor is rigidly mounted to the bottom of the steering column through a coupler, which is a connector between the motor shaft and the end of the steering column. Through this rigid connection, the steering command from steering wheel by the operator can be transferred to the DC geared motor as a disturbance to the tactile feedback control system and the resistant torque of the motor which is regulated by the tactile feedback controller output voltage can be relayed to the operator through the steering column. To minimize the backlash in the system, a good positive engagement in the coupler between the steering column and the DC geared motor shaft is strictly required so that the motor can be mounted accurately to get correct engagement of the gears. If there is slackness between the mating steering column and the DC geared motor shaft, a lose of motion will occur when the movement of the motor is reversed before the contact is re-established. To keep the DC geared motor steady, a motor hanger is made to be mounted to the bottom of the steering column base and the motor is attached to the motor hanger to keep steady.

The modified steering column is mounted to the cab of the windrower through four holes in the cab floor, as shown in Figure 2.8. This is a picture taken from underneath and in front of the cab. The bottom of the steering shaft will stick down through the hole with wires coming out. The hole is plugged by cloth in the picture. A modified steering column has been mounted to the cab of the windrower which can be seen in Figure 2.7

#### **2.4.4 Pressure Transducers**

Apart from the angle and angular velocity of the steering wheel, the turning status of the vehicle is the other part of the input signals to the tactile feedback controller. The turning status of the vehicle is provided by measuring relative hydraulic pressures of both the left and the right side of the hydraulic driving system down in



**Figure 2.7:** A modified steering column has been mounted to the cab of the prototype windrower.

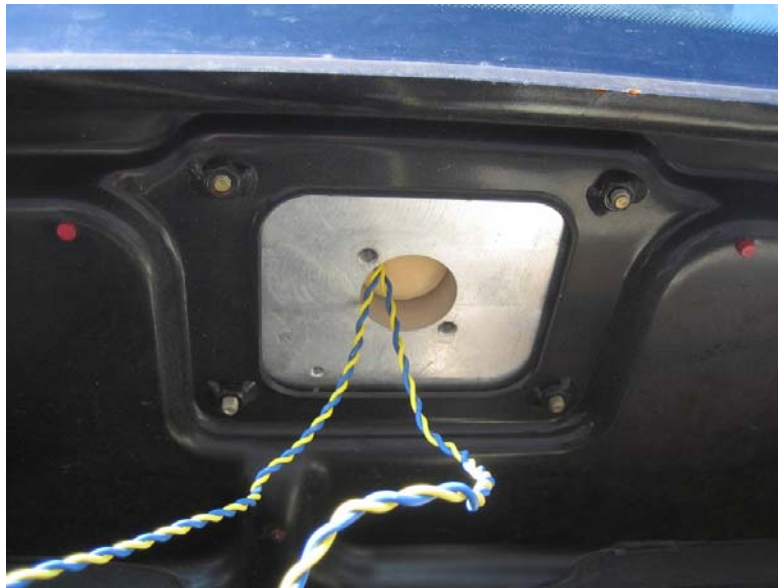


**Figure 2.8:** A picture taken from underneath and front of the cab to show how the steering column attaches to the cab of the windrower through the hole on the cab floor.

the pipelines. The relative hydraulic pressures on both sides are measured with pressure transducers. A pressure transducer is a transducer that converts pressure into analog electrical signal. Although there are various types of pressure transducers, one of the most popular ones is the strain-gage based transducer. The conversion of pressure into electrical signal is achieved by physical deformation of strain gages which are bonded into the diaphragm of the pressure transducer and wired into a Wheatstone bridge configuration. Pressure applied to the pressure transducer produces a deflection of the diaphragm which introduces strain to the gages. The strain will produce an electrical resistance change proportional to the pressure. Pressure transducers generally give an analog electrical output as a voltage or current signal.

In current research, to calculate the vehicle turning status, two pressure transducers are used on both left and right sides of the hydraulic driving system. One is to measure the pressure on the high pressure side of the hydraulic motor and the other is to measure the pressure on the low pressure side of the hydraulic motor. The difference of the high pressure and the low pressure is the relative hydraulic pressure of each side. The output of the pressure transducers used in this project is electrical voltage. The following is the method used in this project to convert the output electrical signals of the pressure transducers to hydraulic pressure. When pressure transducer measured voltage difference is less than or equal to  $0.5 V$ , the relative hydraulic pressure is viewed as 0 Psi. When the voltage difference is greater than or equal to  $4.5 V$ , the relative hydraulic pressure is viewed as 7500 Psi. Voltage difference between 0.5 and 4.5 are linearly interpolated between 0 and 7500 Psi. By comparing the relative hydraulic pressure on the left side and the right side, the turning status of the vehicle can be obtained.

## 2.5 Tactile Feedback Device Electronic Controller

### 2.5.1 Input Circuits

Tactile feedback devices that provide input signals for the tactile feedback controller are connected to different XCM input connectors depending on the form of these input signals. The connections have been designed and necessary modifications for the XCM connector circuits have been made. The pressure transducers provide analog voltage signals, thus they are connected to the analog input connectors of the XCM. The quadrature encoder outputs the numbers of pulses per 10 milliseconds of each channel, so the channels are connected to the frequency input connectors of the XCM. The angle and angular velocity and their directions of the encoder are calculated in the controller according to the channels. For feedback control, the output current of the DC geared motor is connected to the current sense input connectors of the XCM as part of the controller input signals. What is tricky here is that current sensing circuit of the XCM needs to be tuned to adapt to the load device on the circuit which is the DC geared motor in current research. In this application the current sensing circuit of XCM is modified according to the DC geared motor's resistance of coils and the maximum current draw under normal operation conditions. From the experiment the peak current of the DC geared motor under normal operation conditions is 9 A, thus the current sense circuits are configured for a measurement range of 0 to 9 A. The current sense circuits work off 10-bit AtoD converters. Therefore the resolution is the peak current of the DC geared motor divided by 1023 ( $2^{10} - 1$ ) or the resolution is approximately 9 mA per digit which provides sufficiently accurate measurements for the controller. This is enough for the control algorithm. The program related to current control also needs to be changed accordingly. The software architecture for current control including the mathematical model of the plant was built first and then the control gains for the current control circuit are fine tuned.

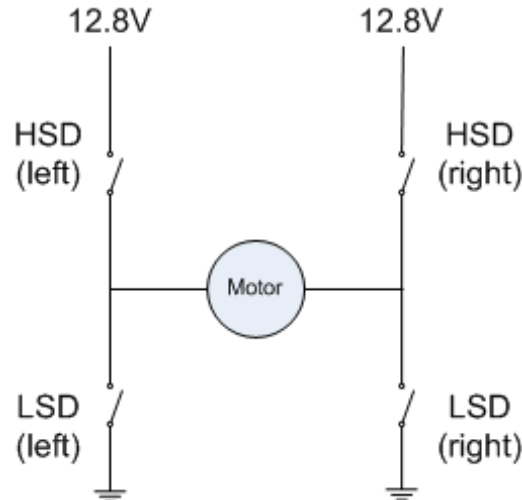


**Figure 2.9:** An illustration of H bridge which is used to achieve both clockwise and counter-clockwise spin of DC motor in the control process.

### 2.5.2 H-bridge to Drive DC Motor

Since steering wheel should be turned in both clockwise and counter-clockwise directions during driving, consequently the DC geared motor needs to be driven in both forward and reverse directions. A very popular circuit that can meet this requirement is called an H-bridge which is shown in Figure 2.9. An H-bridge is built with four controllable switches. When the left high side driver (HSD) and right low side driver (LSD) are closed and right HSD and left LSD are open, a positive voltage will be applied across the motor. By opening left HSD and right LSD and closing right HSD and left LSD, the applied voltage is reversed, allowing the reverse rotation of the motor. Left HSD and left LSD should never be closed at the same time, as this would cause a short circuit on the voltage source. The same rule applies to right HSD and right LSD.

The XCM have been modified by integrating an external H-bridge to realize reversible rotation of the DC geared motor. The Pulse-Width-Modulation (PWM) voltage which switches between 0 V and 13.8 V is produced by the tactile feedback

controller to drive the DC geared motor. Relays have been used as the controllable switches of the external H-bridge. The PWM voltage is applied to one input or the other based on the desired rotation direction of the DC geared motor. This is controlled by the micro-computer of the H-bridge. When the motor rotation direction needs to be reversed, the switching time from one input of the H-bridge to the other would be approximately 20 ms. Thus it will take about 20 ms for the electric current to switch the motor and steering wheel turning directions. This is fast enough for the steering wheel to turn directions during driving an agriculture machine because the nature of human being operation is slow.

## Chapter 3

### SYSTEM MODELING

#### 3.1 Introduction

To design the tactile feedback control algorithm, system modeling of the tactile feedback hardware system is required. System modeling or known as system identification involves estimating impulse response or transfer function of a system from its input and output measurements. In this chapter adaptive filters are used for tactile feedback hardware system identification, which is a filter that self-adjusts its transfer function by an optimization algorithm according to the system input and output. In current research a linear adaptive filter whose block diagram is shown in figure 3.1 is developed. In current system identification, the input signal and the desired response of the filter is available. So Least Mean Squares (LMS) algorithm is used for the adaptive filter as the optimization algorithm to find the filter coefficients. In this way the filter produces the least mean squares of the error signals which are the difference between the desired and true outputs. LMS is a stochastic gradient descent method in that the filter is only adapted based on the error at current time. LMS algorithm is one of the method to identify the unknown system  $h(n)$  by adapting the filter  $\hat{h}(n)$  to make it as close as possible to  $h(n)$ , using only observable signals  $x(n)$ ,  $d(n)$  and  $e(n)$ . The structure of the system model is selected based on its theoretical model structure which is described below.

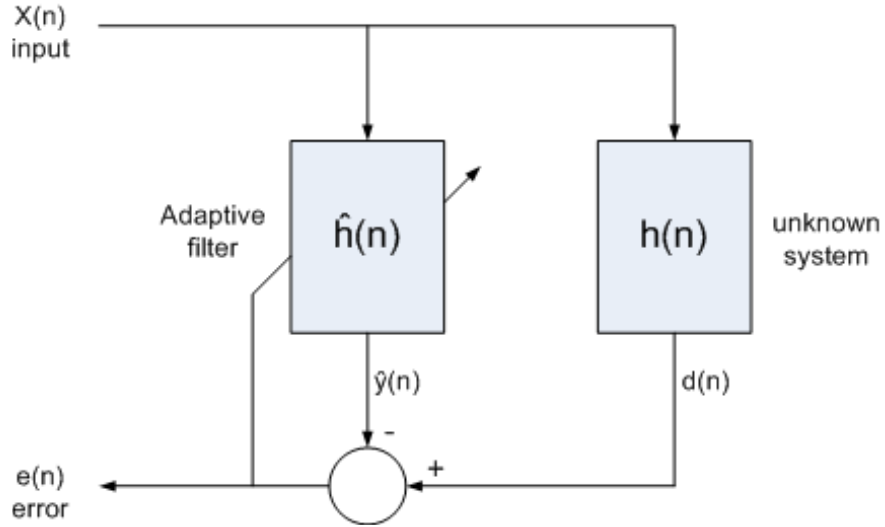


**Figure 3.1:** Block diagram of adaptive filter used for system identification.

### 3.2 Theoretical Model of the Steering Control System

The steering control system consists of a tractor steering column driven by a DC geared motor. The DC motor is the key component of this system. Its equivalent electric circuit is shown in figure 3.2.  $e$  is the back emf (electromotive force), which is the generated voltage counters the applied voltage and is proportional to the motor's angular velocity. Its value can be calculated with Equation (3.1), where  $K_e$  is the electric constant. An electric current  $i_a$  flows through the DC motor's armature with a value determined by the applied voltage  $V_a$ , the motor's inductance  $L_a$ , resistance  $R_a$  and back emf voltage  $e$ . The relations can be expressed in Equation (3.2).

$$e = K_e \dot{\theta}. \quad (3.1)$$

$$V_a - e = L_a \frac{di_a}{dt} + R_a i_a. \quad (3.2)$$

The mechanical components of the system can be modeled as a turning shaft with moment of inertia  $J_m$  and viscous friction coefficient  $b$ . The DC motor converts

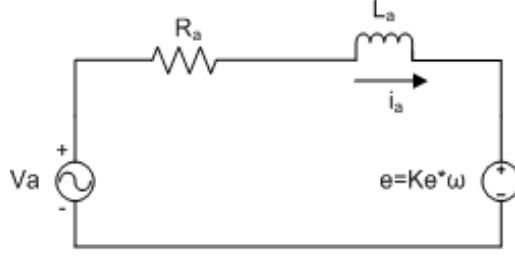


**Figure 3.2:** Diagram of equivalent electric circuit of a DC motor.

the electric armature current into a mechanical torque  $T$  that is applied to the shaft, which couples the electric DC motor and the system mechanical components, as expressed in Equation (3.3).

$$T = K_t i_a. \quad (3.3)$$

When a driver operates on a steering column system, the driver applied torque and motor generated torque produce an angular velocity  $\omega = \dot{\theta}$  according to the moment of inertia  $J_m$  and viscous friction of the system as shown in Equation (3.4):

$$T + T_h = J_m \ddot{\theta} + f(\dot{\theta}), \quad (3.4)$$

where  $J_m$  is the rotational inertia of the steering column,  $T_h$  is the disturbance caused by the operator, and  $f(\dot{\theta})$  is the damping in the system.  $f(\dot{\theta})$  consists of friction and viscous damping and is usually unknown. Likewise, the disturbance torque  $T_h$  represents human-machine interaction and also is an unknown quantity.

### 3.3 Motivation for System Identification

It is of great importance to model the plant of a control system for control algorithm design. For the tactile feedback control of steer-by-wire agriculture machine, the objective is to control the angle and the angular velocity of the steering column. Although the structure of the system's theoretical model has been given, it is difficult to use this theoretical model structure to obtain the plant model here.

First there are some quantities which are hard to know. For instance, the disturbance torque  $T_h$  is unknown because of the uncertainty of operator's impact on the steering wheel and the difficulty of measuring torque directly. Another quantity that is difficult to know is the friction and viscous damping of the system  $f(\dot{\theta})$ . Another reason for the necessity of system identification is some system parameters, such as inductance and resistance of the DC motor are changing with variation of the environment. It is necessary to perform adaptive modeling to get a realistic model of the system. Furthermore the modeling eliminated the boring task of measuring moment of inertia of the irregular shaped system.

The steps of identifying steering column system is as follows. First, we need to design an experiment to acquire input and output signals of the system. Second, we need to analyze the signals and choose a suitable modeling method based on the analysis. Third, according to the modeling result, some modeling improvement may be needed, such as updating algorithm or further study of the model.

### 3.4 A Review of Digital Filters

In this section, two types of digital filters which are candidates for tactile feedback system identification are reviewed. They are finite impulse response (FIR) filter and infinite impulse response (IIR) filter. FIR filter is defined by the difference equation (3.5).

$$y(n) = \sum_{i=0}^N h(i) x(n-i), \quad (3.5)$$

where  $x(n-i)$  is the input signal of the previous  $i$ th step. When  $i=0$ , it stands for the current step input signal.  $y(n)$  is the current step output signal and  $h(i)$ 's are the filter coefficients.  $N$  is known as the filter order and an  $N^{th}$ -order filter has  $(N+1)$  terms on the right-hand side which are commonly referred to as taps. The

above filter is a  $N + 1$ -tap filter. The IIR filter is defined by equation (3.6).

$$y(n) = \sum_{i=0}^P b(i) x(n-i) + \sum_{j=1}^Q a(j) y(n-j), \quad (3.6)$$

where  $x(n-i)$  is the input signal of the previous  $i$ th step. When  $i = 0$ , it stands for the current input signal.  $y(n)$  is the current output signal.  $b(i)$ 's are the feedforward filter coefficients and  $a(j)$ 's are the feedback filter coefficients.  $P$  is the feedforward filter order and  $Q$  is the feedback filter order.

Digital filters can give results superior to those of analog filters in almost all areas. With digital filters we can create nearly flat passbands, almost vertical transition bands, and close to ripple-free stopbands. FIR and IIR filters are the two most commonly used digital filters. Which of the two filters should be adopted depends on the frequency spectrum of the data to be processed, the filter weight vector convergence rate, and so forth.

### 3.4.1 System Parameter Identification Using FIR Filter

The response of an FIR filter to an impulse ultimately settles to zero because there is no feedback in the filter. If the input is an impulse, that is, a single "1" sample followed by a sequence of "0" samples, then the output will eventually settle down to zero. This is in contrast to IIR filters which have internal feedback and may continue to respond infinitely.

If the input signal is the Kronecker delta impulse, that is,  $x(n) = \delta(n)$ , the Z-transform of the output  $y(n)$  yields the transfer function of FIR filter which is expressed in equation (3.7).

$$H(z) = \sum_{i=0}^N h(i) z^{-i}. \quad (3.7)$$

From equation (3.7) we can see the transfer function of FIR filter only has zeros but does not have any pole. Therefore FIR filters are clearly Bounded Input Bounded

Output (BIBO) stable. As we can see, the output is the sum of a finite number of finite multiples of the input values, so it can't be greater than  $\sum h(i)$  times the largest input value.

To identify the steering column system, we want to obtain the relation between the system's applied input voltage and its output angular velocity. When an FIR adaptive filter is used, it will give an output  $\hat{\omega}(n)$  which is shown in equation (3.8) to emulate the true output angular velocity.

$$\hat{\omega}(n) = \hat{h}(0)V(n) + \hat{h}(1)V(n-1) + \dots + \hat{h}(N)V(n-N), \quad (3.8)$$

where  $V(i)$  is the applied voltage on the  $i$ th step,  $\hat{\omega}(n)$  is the estimated output angular velocity by the FIR filter and  $\hat{h}(i)$ 's are the filter coefficients. The error between true and estimated output angular velocity is expressed as  $e(n)$  which is shown in equation (3.9).

$$\begin{aligned} e(n) &= \omega(n) - \hat{\omega}(n) \\ &= \omega(n) - \hat{h}(0)V(n) - \hat{h}(1)V(n-1) - \dots - \hat{h}(N)V(n-N). \end{aligned} \quad (3.9)$$

The cost function  $J_n$  is defined as half of the error square in every step by equation (3.10).

$$J_n = \frac{1}{2}e^2(n). \quad (3.10)$$

The idea behind Least Mean Squares filters is taking  $e^2(k)$  itself as an estimate of its mean value and then use steepest descent method to find a coefficient vector  $\hat{h}(i)$  which minimizes the cost function  $J_n$ . The steepest descent direction is the opposite direction of gradient. At each iteration of the adaptive process, the gradient of  $J_n$  can be estimated by Equation (3.11).

$$\begin{aligned} \nabla J_n &= \left[ \frac{\partial J_n}{\partial \hat{h}(0)}, \frac{\partial J_n}{\partial \hat{h}(1)}, \dots, \frac{\partial J_n}{\partial \hat{h}(N)} \right] \\ &= [-e(n)V(n), -e(n)V(n-1), \dots, -e(n)V(n-N)]. \end{aligned} \quad (3.11)$$

The steepest descent direction of  $J_n$  is  $-\nabla J_n$ , so with LMS adaptive algorithm,  $\hat{h}(i)$  is updated by equation (3.12).

$$\hat{h}(i+1) = \hat{h}(i) + \mu_i e(i) V(i), \quad (3.12)$$

where  $\mu_i > 0$  is the step length that regulates the speed and the stability of adaptation.

FIR filter is widely used because of its several useful properties. First, FIR filter is easy to implement and have a simple numerical property because its output is a linear combination of its previous and current inputs and feedback is not used. The filter is memoryless of past numerical errors, so any rounding error will not be cumulated by summed iterations and the same relative numerical error of implementing FIR filter occurs independently with each calculation. Because of no feedback, FIR filter can be implemented with fewer bits of computation components. Secondly, because there is no feedback in FIR filter, FIR filter is computationally efficient. It is unlike IIR filter in which every output must be calculated to contribute to the feedback. Third, as afore mentioned, FIR filter is inherently BIBO stable, but IIR filter is not.

### 3.4.2 System Parameter Identification Using IIR Filter

The response of an IIR filter to an impulse may continue infinitely because IIR filters have internal feedback. The primary advantage of IIR filters over FIR filters is that they typically meet a given set of specifications with a much lower filter order than a corresponding FIR filter. Moreover, IIR filters are more suitable for modelling resonant systems due to their pole-zero structure. But the inner feedback of IIR filter may cause system instability and complex computation because the IIR filter is influenced by its past output which should be counted for every iteration for the estimation of future response. IIR filter also retains the memory of past

numerical errors and rounding errors may be combined by summed iterations, thus IIR filter needs to be implemented with more bits of computation components.

In current system identification, the IIR filter coefficients are updated on line with the steepest descent adaptation. The estimated output of the next step produced by the IIR filter is to emulate the true output angular velocity. For simplicity, we assume both the feedback and the feedforward terms are of second order, which is sufficient shown below, then  $\hat{\omega}(k)$  is given by equation (3.13)

$$\hat{\omega}(k) = \hat{b}_0(k)\omega(k-1) + \hat{b}_1(k)\omega(k-2) + \hat{a}_0(k)V(k) + \hat{a}_1(k)V(k-1), \quad (3.13)$$

where  $V(k)$  and  $V(k-1)$  are input signals of current and previous stages,  $\omega(k-1)$  and  $\omega(k-2)$  are the output signals in the previous two stages which have been feedback to the filter input to determine the current output with current and previous stages of input signals, and  $\hat{b}_1, \hat{b}_0, \hat{a}_1, \hat{a}_0$  are the estimated filter coefficients.

The signal error  $e(k)$  which is defined as the difference between the desired output and the estimated output is expressed by equation (3.14).

$$\begin{aligned} e(k) &= \omega(k) - \hat{\omega}(k) \\ &= \omega(k) - \hat{b}_0(k)\omega(k-1) - \hat{b}_1(k)\omega(k-2) \\ &\quad - \hat{a}_0(k)V(k) - \hat{a}_1(k)V(k-1). \end{aligned} \quad (3.14)$$

To implement the LMS algorithm, take  $e^2(k)$  in each step as an instantaneous estimation of its mean value and define the cost function as half of the square error in every step which is shown in equation (3.15).

$$J_k = \frac{1}{2}e^2(k). \quad (3.15)$$

To minimize the cost function  $J_k$ , the steepest descent method is used. The gradient of  $J_k$  is given by equation (3.16) and the search direction is  $-\nabla J_k$ .

$$\begin{aligned} \nabla J_k &= \left[ \frac{\partial J_k}{\partial \hat{b}_0}, \frac{\partial J_k}{\partial \hat{b}_1}, \frac{\partial J_k}{\partial \hat{a}_0}, \frac{\partial J_k}{\partial \hat{a}_1} \right] \\ &= [-e(k)\omega(k-1), -e(k)\omega(k-2), -e(k)V(k), -e(k)V(k-1)]. \end{aligned} \quad (3.16)$$

With this estimation of gradient, the LMS adaptive iteration can be specified by equation (3.17)

$$\begin{aligned}
 \hat{b}_0(k+1) &= \hat{b}_0(k) + \mu_{b0}e(k)\omega(k-1) \\
 \hat{b}_1(k+1) &= \hat{b}_1(k) + \mu_{b1}e(k)\omega(k-2) \\
 \hat{a}_0(k+1) &= \hat{a}_0(k) + \mu_{a0}e(k)V(k) \\
 \hat{a}_1(k+1) &= \hat{a}_1(k) + \mu_{a1}e(k)V(k-1).
 \end{aligned} \tag{3.17}$$

where the step length  $\mu_{b0} > 0$ ,  $\mu_{b1} > 0$ ,  $\mu_{a0} > 0$  and  $\mu_{a1} > 0$  regulate the speed and stability of the adaptation.

### 3.5 Data Acquisition

The first step of tactile feedback hardware system identification is to acquire the input and output signals of the system. The signals to be acquired are the voltage applied to the DC geared motor, the electric current which goes through the DC geared motor and the pulse number per 10 milliseconds of the encoder's channel A or channel B. Because of the existence of back emf, the applied voltage is different from the voltage measured on the motor. The applied voltage is provided by a PWM power source of 13.8 V with varying duty cycle. So, to obtain the exact applied voltage, the duty cycle of the PWM power source is a parameter to be measured.

System signals are processed by the microcontroller XCM. The designed experiment circuit diagram is shown in Figure 3.3. In the experiment circuit, two parallel connected HSDs (High Side Drivers) work as the power source and the voltage is 13.8 V. Two parallel connected HSDs are used to allow bigger permitted electric current through the circuit. The actual applied voltage to the DC geared motor is controlled by a potentiometer whose value reads through the XCM by connecting to one of its analogue input connectors. The electric current that goes

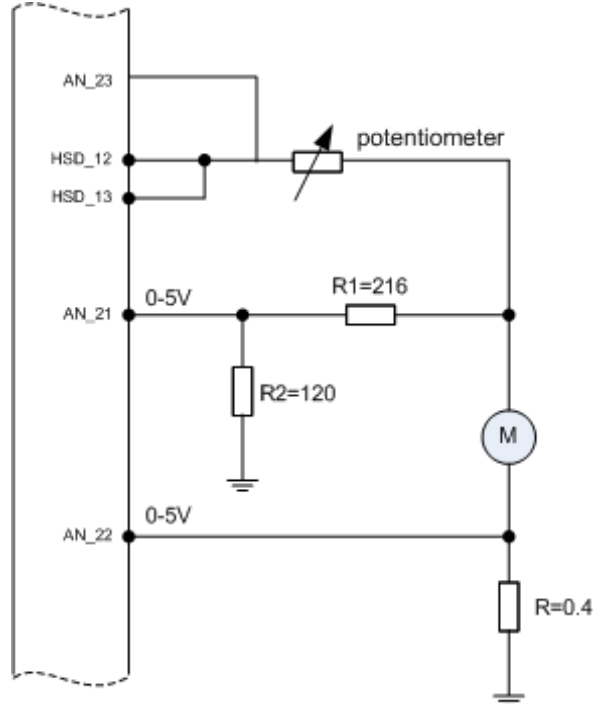


**Figure 3.3:** The electric circuit diagram for data acquisition of steering column system identification experiment.

through the DC geared motor is not easy to measure directly, so instead we calculate the electric current of a known value resistance that is serially connected to the DC geared motor. The voltage of the resistance is fed through an Analogue Input of XCM. The voltage of the DC geared motor is also measured for reference. The maximum measured voltage should be close to  $13.8\text{ V}$  which is the voltage of the PWM power source. But the Analogue Inputs can only read a maximum voltage of  $5\text{ V}$ , so a voltage divider is used to measure part of the voltage and then the whole voltage is calculated.

To make it clear, a simplified version of the electric circuit is given in figure 3.4. The selection of resistances is a trial and error process. First, we want  $V_1$  to be negligible so that the voltage obtained by adjusting the potentiometer can be

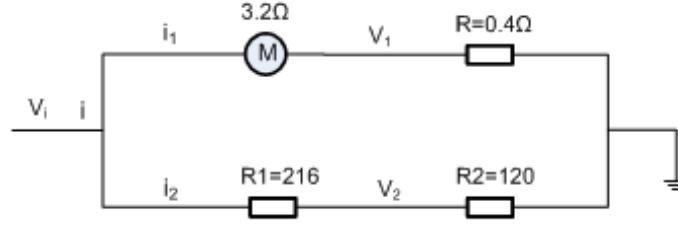


**Figure 3.4:** A simplified version of the electric circuit for data acquisition of steering column system identification experiment.

considered as the applied voltage to the DC geared motor. So the resistance  $R$  needs to be as small as about  $\frac{1}{10}$  of the nominal resistance of the DC geared motor which is  $3.2 \Omega$  (rounded from the nominal resistance of  $3.2155 \Omega$ ). Restricted by the availability of small value resistance,  $R$  is chosen to be  $0.4 \Omega$  which is a little bit bigger than  $\frac{1}{10}$  of the motor resistance. Second, the maximum  $i_1$  are designed to be as big as possible so that the DC geared motor can produce possible maximum output torque.  $R_1 + R_2$  are decided to be chosen around 10 times of the motor resistance. To make sure  $V_2$  is no more than  $5 V$ , we assumed that  $V_2 = 5 V$  when  $V_i = 14 V$ , then the ratio  $R_1/R_2$  is calculated by equation (3.18) and the result is  $R_1/R_2 = 1.8$ .

$$5 = 14 \frac{R_2}{R_1 + R_2}. \quad (3.18)$$

By trial and error,  $R_2 = 120 \Omega$  and  $R_1 = 216 \Omega$  have been chosen. The total resistance of  $R_1$  and  $R_2$  is  $336 \Omega$ , which qualifies the requirement that it is around 10 times of the DC geared motor resistance.

After all needed information has been put into XCM, Controller-Area-Network (CAN) bus is used for data acquisition purposes. Data of interest are put into a CAN message and broadcast onto the CAN bus. CANalyzer is the software tool to be used to log the CAN messages on a laptop PC and plot the data diagram.



**Figure 3.5:** A picture of the testbed for data acquisition of steering column system identification experiment.

The testbed of steering column system identification data acquisition can be seen in Figure 3.5.

### 3.6 Data Analysis and Model Selection

Figure 3.6 shows the diagram of the voltage duty cycle applied to the steering column system. Figure 3.7 is the diagram of pulse count per 10 ms of encoder channel A. We can see small teeth on the curves in both Figures caused by noise involved in the signals during data acquisition. To get rid of the noise and smooth the curves, the data are averaged on an interval of ten data points which means the average of the first ten data is calculated to be the first data and the second to the eleventh

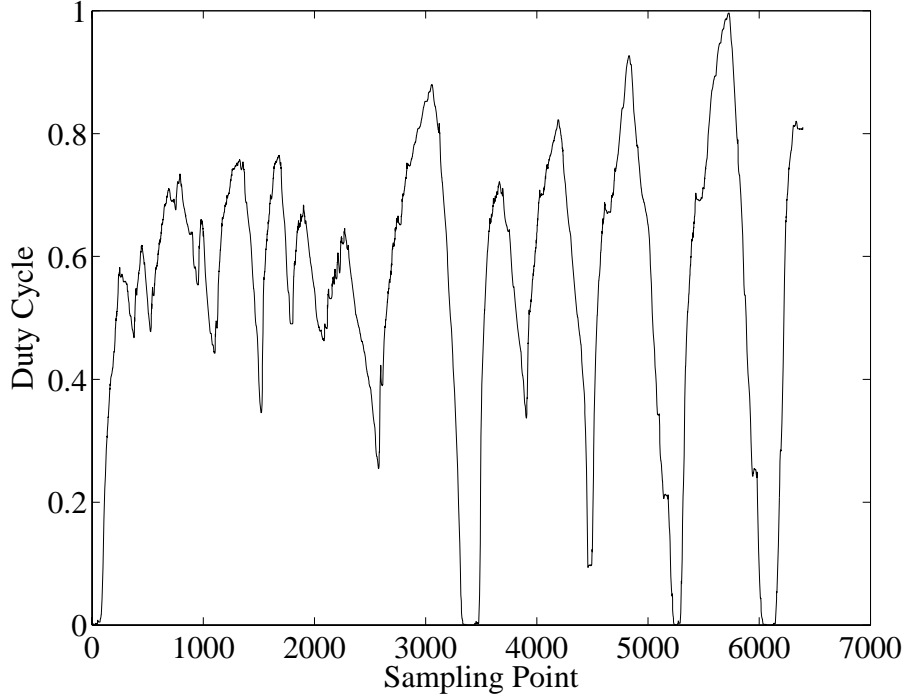


**Figure 3.6:** Voltage duty cycle applied to the steering column system. This reflects the real voltage input to the system.

data are averaged to be the second data, etc.

The true voltage applied to the system is calculated by equation (3.19).

$$V_{app} = V_T d_c, \quad (3.19)$$

where  $V_{app}$  is the voltage applied to the steering column system,  $V_T$  is the constant power supply provided by XCM and its value is  $13.8V$ , and  $d_c$  stands for the duty cycle of the Pulse-Width-Modulated (PWM) power supply. The output angular velocity of the steering column is calculated by equation (3.20).

$$\omega_{sys} = \theta_A N_A / T_{step}, \quad (3.20)$$

where  $\omega_{sys}$  is the angular velocity of the steering column,  $N_A$  is the pulse count per 10 ms of encoder channel A,  $T_{step}$  is the time period in which the encoder pulse is

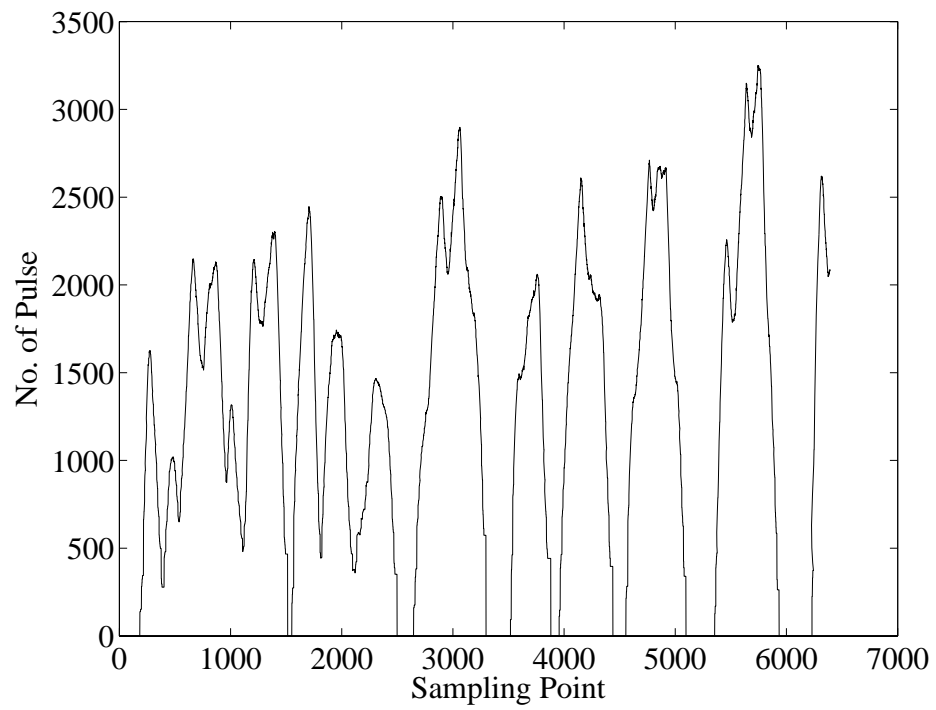


**Figure 3.7:** Pulse count of encoder channel A in every 10 milliseconds.

counted and  $T_{step}$  equals 10 ms here,  $\theta_A$  is the resolution of the encoder, which is the angle turned corresponding to one pulse count of the encoder. The encoder used in this project has a resolution of 400 count per revolution (CPR), so

$$\theta_A = 2\pi/400. \quad (3.21)$$

Spectrums of the system input and output signals have been analyzed with Fast Fourier Transform (FFT) method. The input signal spectrum is shown in figure 3.8 and the output signal spectrum is shown in figure 3.9. From the spectrums we can see that both input and output signals have a single main frequency that is close to 0 because the DC geared motor is a low pass filter. Bode plot of the steering column system in figure 3.10 reveals that the nature of the system is of low order and there is no resonance in the system.

## 3.7 System Modeling

### 3.7.1 Model Selection

Although the theoretical model of the tactile feedback hardware system is not easy to use for system identification, a general idea of the system model structure can be inferred based on that. From the theoretical model structure, it is known without difficulty that the model is of low order. Because the mechanical and electrical components of the system are both of second order, the order of the coupled model will be no more than four. To identify the tactile feedback hardware system, FIR and IIR models of order four or less are fitted to find the most suitable model. In real time adaptive process, the weight vector of digital filter is updated by equation (3.12) for FIR filter and by equation (3.17) for IIR filter. All the filters adapt twice. The first adaptation is nonadaptively iterated and the second adaptation is adaptively iterated in which the estimated output angular velocity is recalculated in synchronization with the updated weight vector. The non-adaptive adaptation generated weight is made the initial weight value of the adaptive adaptation. In the

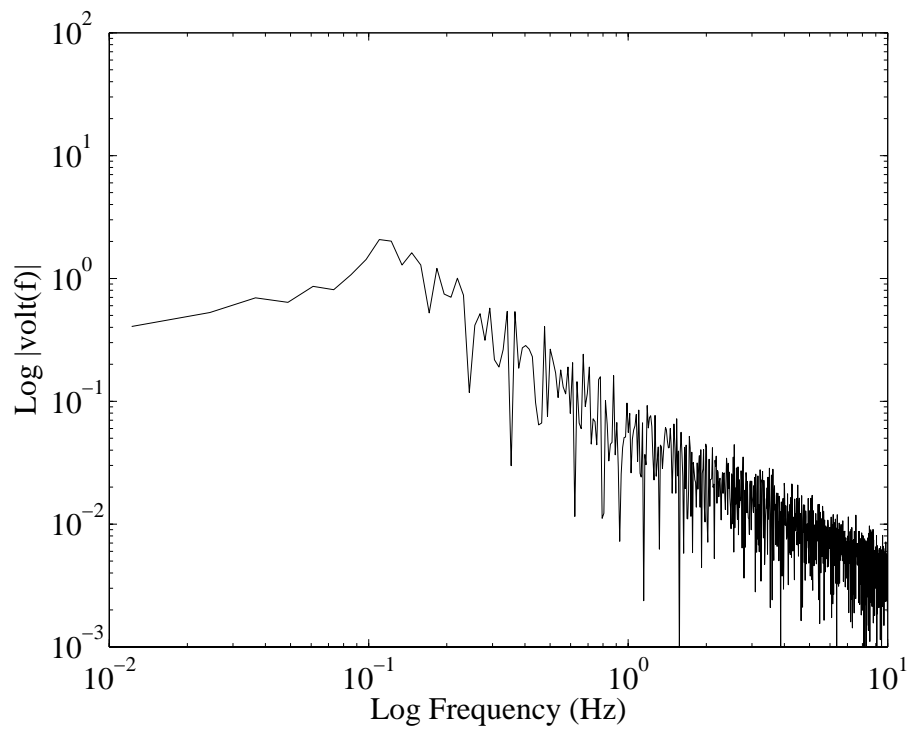


**Figure 3.8:** Spectrum of steer-by-wire system input voltage.

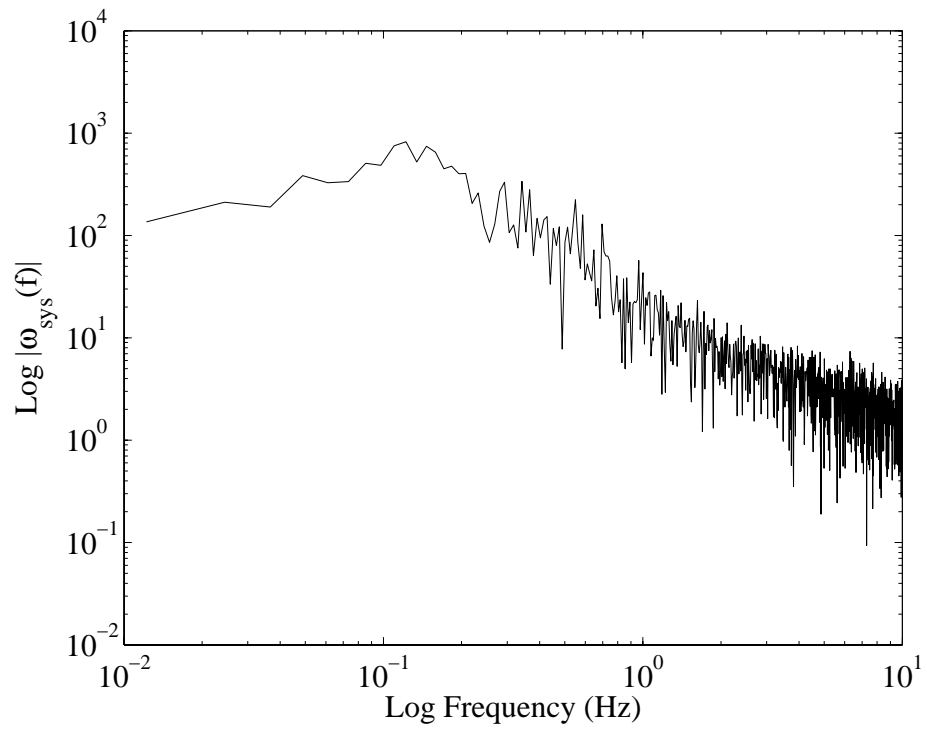


**Figure 3.9:** Spectrum of steer-by-wire system output angular velocity.

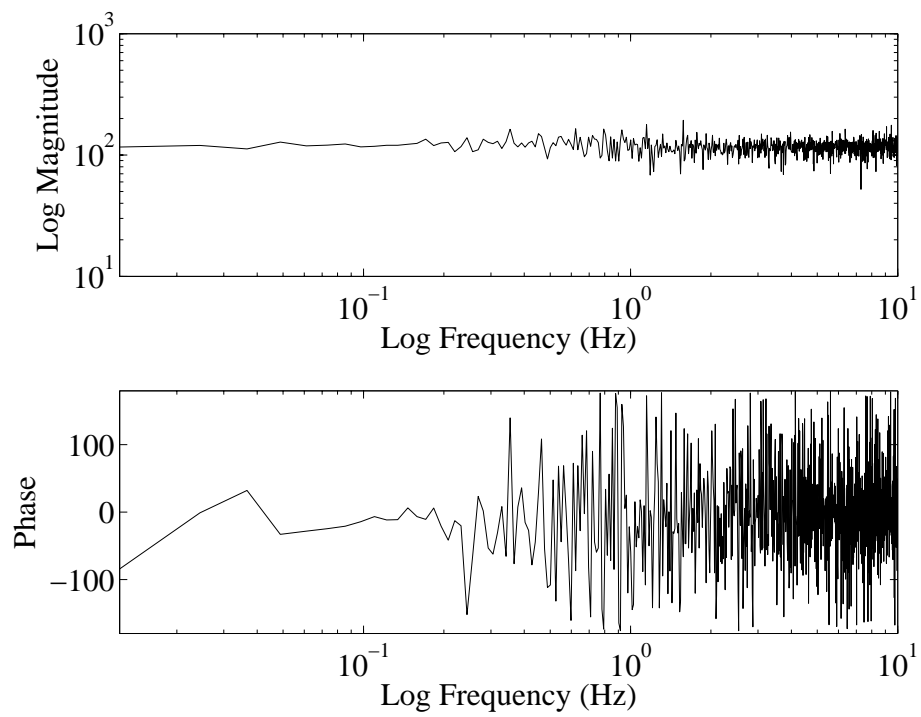


**Figure 3.10:** A Bode plot of steer-by-wire system transfer function.

adaptive adaptation the weight vector is updated every 5 steps instead of every step which reduces the amount of calculation considerably while still achieving sufficient accuracy. In every 5 steps, the weight vector will stop updating till the weights have no significant change which means the change of the weight in two sequential iterations is less than 5%. Defined by the designed algorithm, the minimum iteration time is 10 and the maximum iteration time is 100.

Root mean squares of the errors are calculated and plotted for all of the fitted FIR and IIR models to evaluate the selected model. From figure 3.11, we can see that as the order increases the error between true and generated signals decreases monotonically. IIR filters have relatively smaller error than that of the FIR filters of the same order, but there is no big difference between FIR and IIR filters if the order is 2 or higher. Although FIR filter have the advantages of being simple and efficient, the weight vector of the FIR filters does not converge fast enough. Thus, an IIR filter of order 2 is selected to build the model. The estimated output angular velocity of the steering column system is expressed in equation (3.22) and the IIR filter weight vector converges well. The tactile feedback hardware system transfer function is in the form of equation (3.23).

$$\hat{\omega}(k) = \hat{b}_0\omega(k-1) + \hat{b}_1\omega(k-2) + \hat{a}_0V(k). \quad (3.22)$$

$$\frac{\Omega(z)}{V(z)} = \frac{\hat{a}_0}{1 - \hat{b}_0z^{-1} - \hat{b}_1z^{-2}}. \quad (3.23)$$

To verify the effectiveness of using second order IIR filter to model the tactile feedback hardware system, we compared the output signals of the adaptive filter and the output of the steering column system. From figure 3.12, it is shown that the two signals are coincident well except at some inflexions. The difference of the two signals is within 5% except at the inflexions, which is shown in figure 3.13. At the inflexions the input signal is of high frequency, but in current research, the system

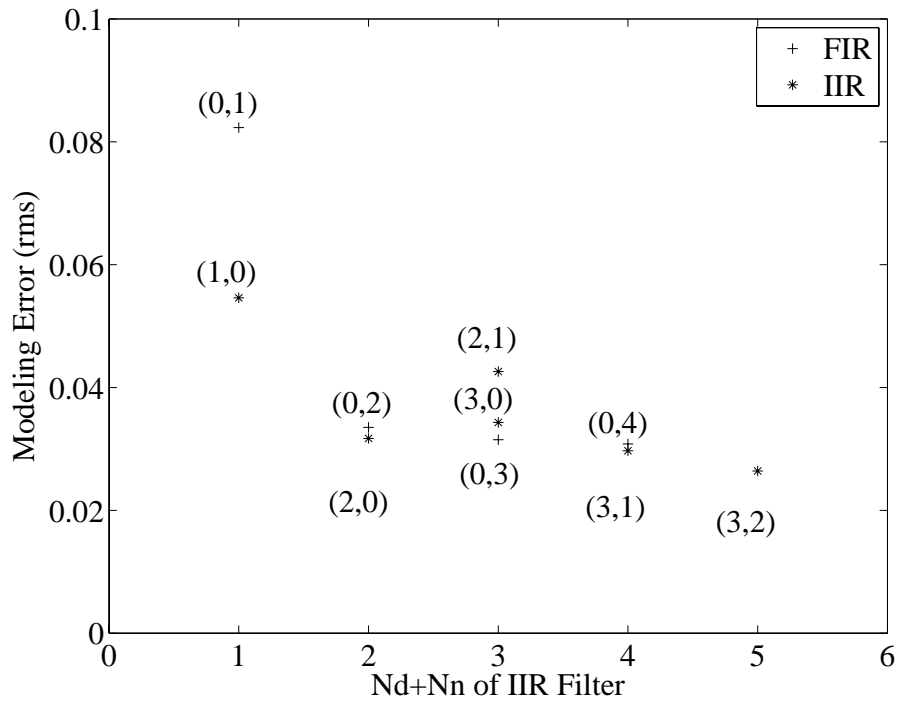


**Figure 3.11:** This is a root mean squares plot of all fitted FIR and IIR models of order 4 and less. It is shown there is no big difference between FIR and IIR filters if the order is 2 or higher.

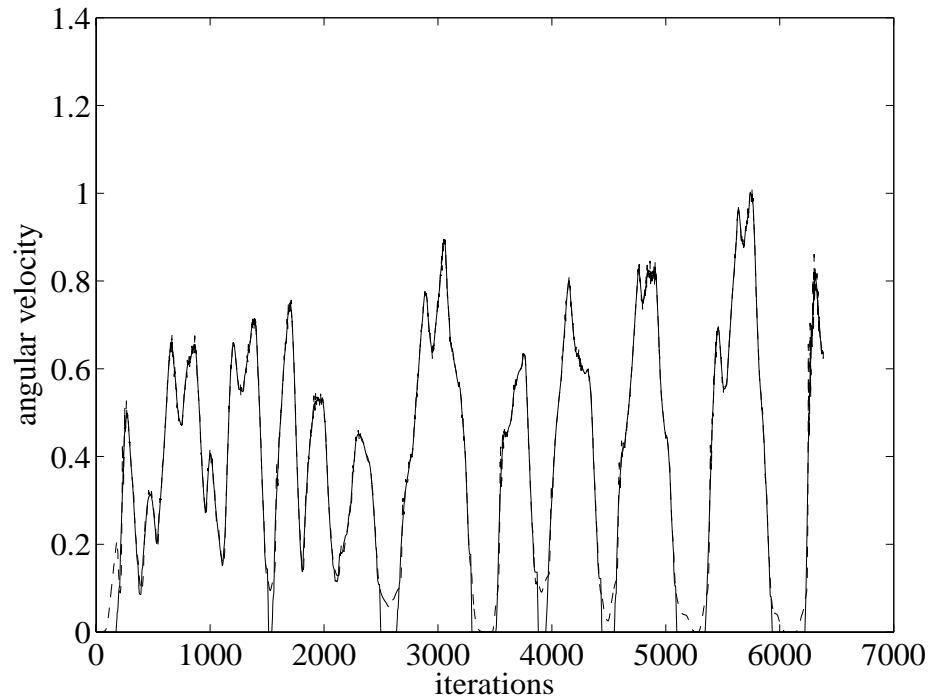


**Figure 3.12:** The output signals of the second order IIR adaptive filter and the steering column system are coincident except at the inflexions.

identification is applied to the steering wheel system of an agriculture machine where it is not likely the input signal is of high frequency, so the poor performance of the IIR filter at the inflexions does not need to be worried and the calculated model will follow the true system well in practice.

### 3.7.2 Convergence of the Mean Weight Vector

As afore mentioned the weight vector is updated according to LMS adaptive algorithm. It is a steepest descent type adaptive algorithm with slow adaptation acting like a low pass filter that ameliorates the effects of gradient estimation noise. No matter FIR filter or IIR filter, the weight vector is updated according to adaptive

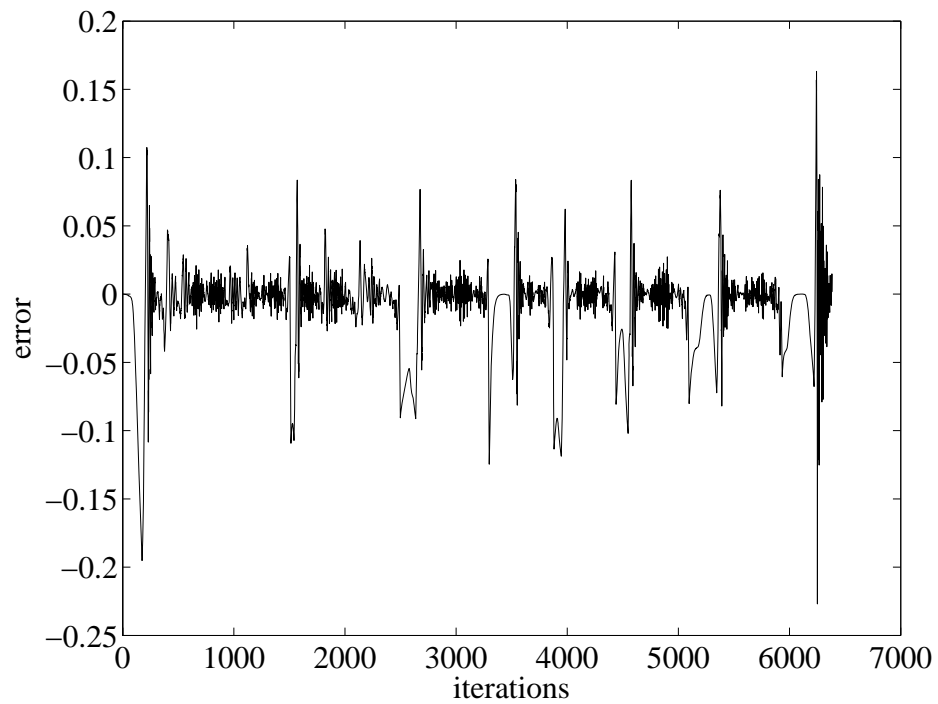


**Figure 3.13:** This diagram shows that the difference between the output signals of the second order IIR adaptive filter and the steering column system is within 5% except at the inflexions.

algorithm expressed in equation (3.24).

$$W(k+1) = W(k) + \mu e(k) X(k), \quad (3.24)$$

where  $W_{k+1}$  is the updated weight vector for next iteration,  $W_k$  is the weight vector of current iteration,  $e_k$  is the error between real signal and filter generated signal at current step.  $X_k$  is the common input signal for both the steering column system and the IIR filter.  $\mu$  is the step length that regulates the speed and stability of adaptation. If successive input signals are independent, after a sufficient number of iterations, the weight vector  $E[W_k]$  converges to  $W^* = E[X_k X_k^T]^{-1} E[d_k X_k]$ , which is the Wiener optimal solution. This convergence is guaranteed only if

$$\frac{2}{\lambda_{\max}} > \mu > 0,$$

where  $\lambda_{\max}$  is the largest eigenvalue of  $E[X_k X_k^T]$ . Here  $\mu_{b0} = 0.009$ ,  $\mu_{b1} = 0.05$  and  $\mu_a = 0.001$ . The weights  $a0$ ,  $b0$  and  $b1$  converge as shown in figure 3.14. The mean values of each weight is  $E[a0] = \hat{a}_0 = 0.0248$ ,  $E[b0] = \hat{b}_0 = 0.1534$ ,  $E[b1] = \hat{b}_1 = 0.7907$ .

### 3.7.3 Transfer Function of the System

Based on the analysis above, the tactile feedback system can be modeled as a second order IIR filter. The parameters have been estimated as  $\hat{a}_0 = 0.0248$ ,  $\hat{b}_0 = 0.1534$  and  $\hat{b}_1 = 0.7907$ . So discrete transfer function of the system is expressed as:

$$\frac{\Omega(z)}{V(z)} = \frac{0.0248}{1 - 0.1534z^{-1} - 0.7907z^{-2}}. \quad (3.25)$$

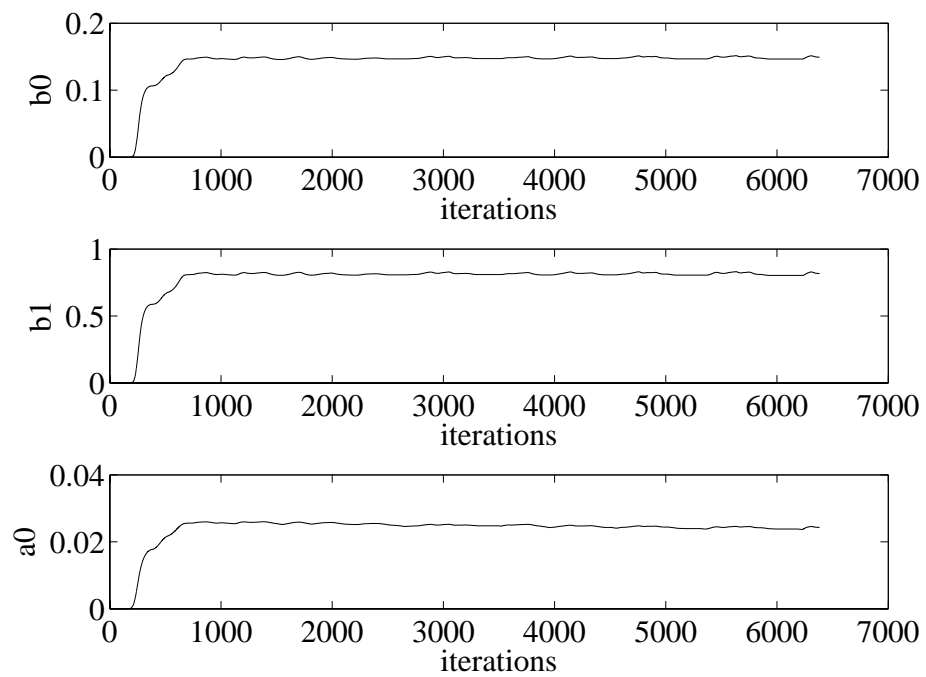


**Figure 3.14:** The weights of the second order IIR filter converge after 1000 iterations.

## Chapter 4

# TACTILE FEEDBACK CONTROL

### 4.1 Introduction

Steer-by-wire device is an electronic control system which replaces the mechanical interface between the driver and the vehicle. A steer-by-wire system can be viewed as a master-slave system, where the tactile feedback part represents the master, and the vehicle propulsion corresponds to the slave. The master and slave are controlled separately and they are coupled by the feedback of the hydraulic signal from the slave to the master.

Because of the lack of mechanical connection between the steering wheel and the propulsion system, the mechanical resistance during operation which provides an intuitionistic signal of the activity of the operator and the response of the vehicle does not exist as in traditional vehicles. Operators of the machine respond with a time delay to the vehicle movement when steering, which makes the operator steer back and forth in an oscillatory manner. To improve the operation of the steer-by-wire vehicle, we need to simulate the mechanical resistance of the conventional steering wheel and front wheel linkage mechanism by means of electronic and feedback control.

### 4.2 Control Architecture

Figure 4.1 describes the control architecture of the steer-by-wire agriculture machine. Turning of the steering wheel sends a command to the control valve which

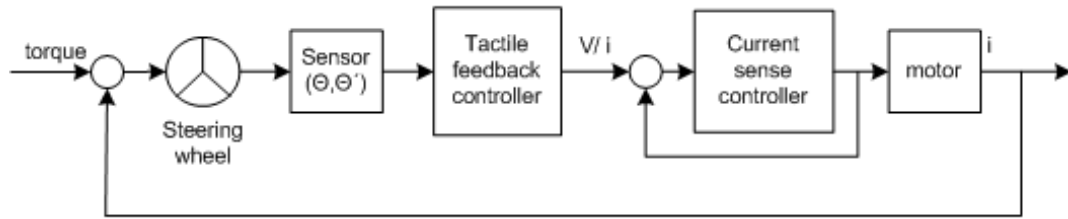


**Figure 4.1:** This chart describes the control architecture of the whole steer-by-wire vehicle system. Tactile feedback controller is used to recover the mechanical linkage resistance. A current sense controller is used to regulate electric current of the DC motor.

splits the power to the wheels of the vehicle. The vehicle turns due to the differentials of the wheel speeds. An optical encoder is used to measure the angle and angular velocity of the steering wheel, and feeds the measurement to the tactile controller. The actuator of the tactile controller is a DC geared motor which provides the mechanical feedback sensation to the operator.

Because the resistance of the motor coil changes with the environment, the electrical current varies even with a constant input voltage. Since the torque of DC motor is proportional to its electrical current, it is important to use a current regulator around the motor.

### 4.3 Current Control

A controller is designed to regulate the electrical current of the DC motor, which compensates for disturbances and variations in the plant. This electrical current regulation is important because when the rotational friction torque is not considered, the output torque of the tactile control is proportional to the current of the DC motor. The primary causes for current variations include back-EMF and temperature. The electrical current of the DC motor is determined by the difference between the applied voltage and the back-EMF divided by the impedance of the DC

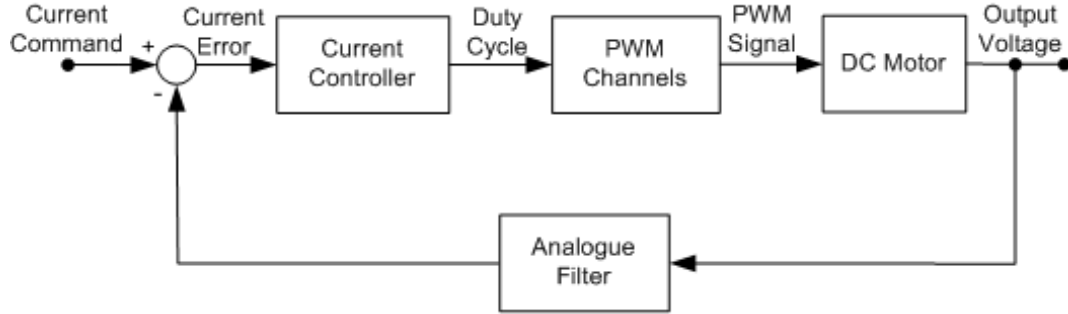


**Figure 4.2:** Block diagram of the current control loop.

motor which consists of the resistance and the inductance of the motor.

A Simulink model of the system is shown in Figure 4.2. Hardware and software features modelled in this system include a pulse-width-modulated (PWM) output driver, a DC motor, an analogue current sensing filter, and a digital controller.

PWM works by high frequency switching between a high voltage and a low voltage. In the current controller design, the PWM runs at 500  $Hz$  switching between 13.8 V and 0 V. The average output voltage is controlled by the amount of time at these voltages. Equation (4.1) shows how the average output voltage is calculated.

$$V_{out} = V_H \left( \frac{t_H}{t_F} \right) + V_L \left( \frac{t_F - t_H}{t_F} \right), \quad (4.1)$$

where  $t_H$  is the time at the high voltage,  $t_F$  is the time of each frame of the duty-cycle and  $0 \leq t_H \leq t_F$ ,  $V_{out}$  is the average output voltage,  $V_H$  is the high voltage and  $V_L$  is the low voltage. The duty-cycle is defined as a percentage by equation (4.2).

$$duty\ cycle = 100 \left( \frac{t_H}{t_F} \right). \quad (4.2)$$

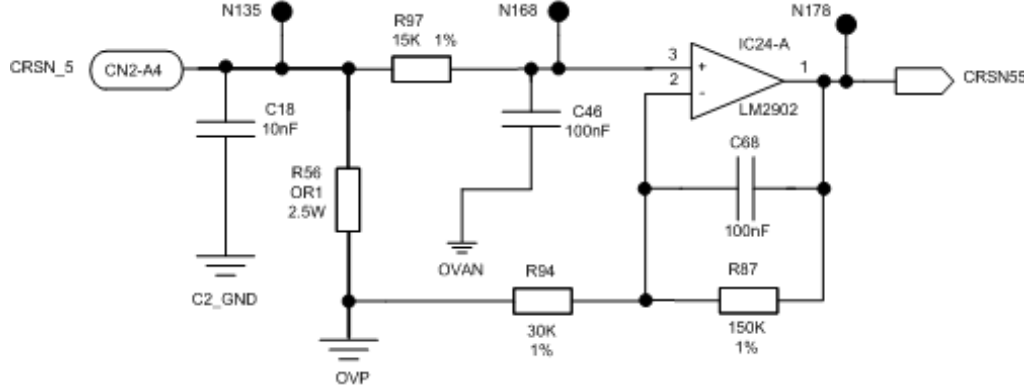


**Figure 4.3:** Circuit diagram of current sensing filter (a second order analogue filter). R56 is the current sensing resistor. The input comes in on CN2-A4 and the output is connected to the 10-bit analogue to digital (A/D) converter at CRSNS5.

A DC motor made by Mabuchi with model number RS-385-SH-2270 has been used as the system actuator. The DC motor electrical circuit is modelled as a resistor, inductor and back-EMF in series. As afore mentioned, the resistance and the inductance of the DC motor vary with time. The nominal resistance is  $3.2155 \Omega$  and the nominal inductance is  $9 \text{ mH}$ . The back-EMF is not considered because the angular velocity of the shaft is low.

The current sensing resistor steps the voltage down and is effectively a voltage divider. The output of the current sensing filter is passed to a 10-bit analogue to digital (A/D) converter. The circuit diagram is shown in Figure 4.3.

The dynamics of the current sensing resistor and the DC motor can be represented by a first order transfer function expressed by equation (4.3).

$$S(s) = \frac{1}{\frac{Ls+R_v}{R_x} + 1} = \frac{11.11}{s + 344.44}, \quad (4.3)$$

where  $L$  is the inductance of the DC motor ( $9 \text{ mH}$ ),  $R_v$  is the resistance of the motor ( $3.215 \Omega$ ) and  $R_x$  is the resistance of the current sensing resistor ( $0.1 \Omega$ , R56 in Figure 4.3). The analogue current sensing filter can be modelled as two separate first order

systems: an input filter ( $F_i(s)$ ) composed of  $R_i$ (R97) and  $C_i$ (C46), and a feedback filter ( $F_{fb}(s)$ ) composed of  $R_{gnd}$ (R94),  $C_{fb}$ (C68) and  $R_{fb}$ (R87).

$$F_i(s) = \frac{1}{R_i C_i s + 1} = \frac{1}{0.0015s + 1}. \quad (4.4)$$

$$F_{fb}(s) = \frac{R_{gnd} R_{fb} C_{fb} + R_{gnd}}{R_{gnd} R_{fb} C_{fb} s + R_{gnd} + R_{fb}} = \frac{450s + 30000}{450s + 180000}. \quad (4.5)$$

Define a second order transfer function  $F(s)$  as,

$$F(s) = \frac{F_i(s)}{F_{fb}(s)} = \frac{667(s + 400)}{s^2 + 733s + 44444}. \quad (4.6)$$

Equations (4.3-4.6) are all in terms of the voltage. To convert the voltage to the current through the sensitivity resistor, we use a gain factor  $K_{v2i}$  as

$$K_{v2i} = R_x \left( 1 + \frac{R_{fb}}{R_{gnd}} \right) = 0.6 \text{ V/A}. \quad (4.7)$$

### 4.3.1 Current Control Algorithm Design

A digital PI controller is designed by using the root locus method. The motor dynamics are included in the root locus but the filter dynamics are excluded. The reason for this is that the filter dynamics are significant faster than those of the motor model. Hence the motor model captures the dominant dynamics of the system. The motor model is converted from the Laplace domain into the discrete time domain using a ‘zero-order’ sampling. The designed controller transfer function is

$$C_i(z) = \frac{K_{p\_i}(z + 0.276)}{z - 1}. \quad (4.8)$$

The closed current loop has a 5% settling time of 0.15sec and a damping ratio of 0.744. Figure 4.4 shows a root locus of the current control system. The zero of the open loop system is at  $z = -0.276$ . The proportional gain is chosen to

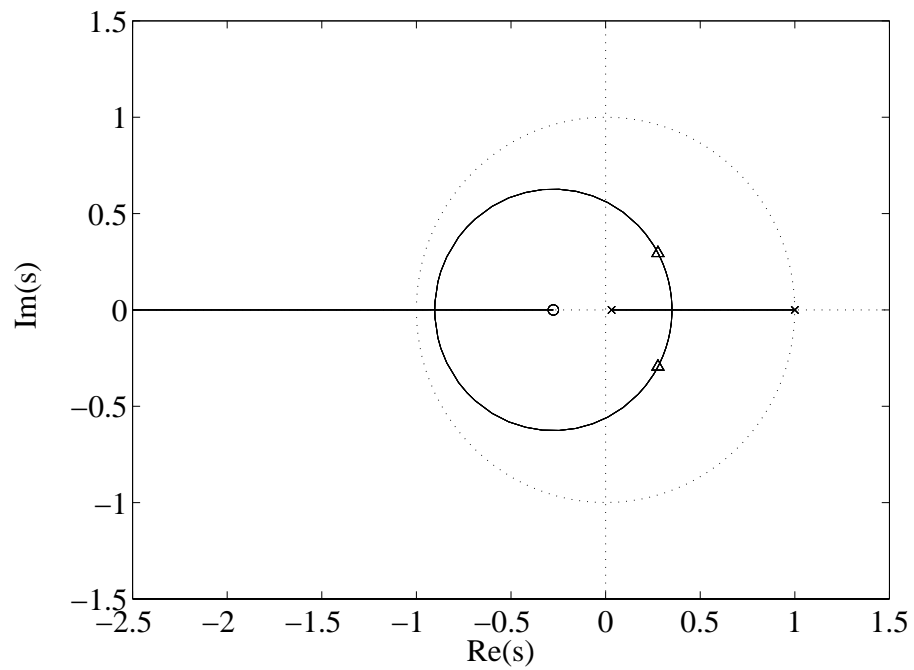


**Figure 4.4:** Root locus of the current control loop. x: Open loop poles. o: Open loop zeros.  $\Delta$ : Closed loop poles at  $z = 0.275 \pm j0.294$ .

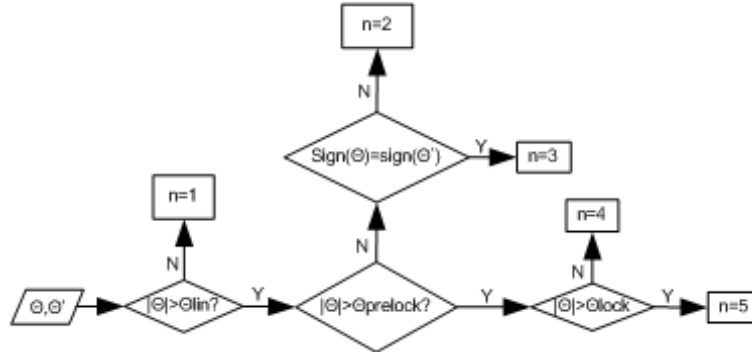


**Figure 4.5:** The switching of different controllers according to the steering wheel angle and angular velocity.

be  $K_{p\_i} = 15.3$ . The closed loop poles of the system indicated by the triangles in Figure 4.4 are  $z = 0.275 \pm j0.294$ . The system is stable when  $0 < K_{p\_i} < 91$ .

#### 4.4 Switching Control

The mechanical resistance is provided by the DC geared motor. The output shaft of the DC motor is rigidly connected to the steering column. When the operator turns the steering wheel, the output shaft of the DC motor is also turned, which provides a disturbance torque to the motor. The controller drives the DC motor to resist the turning of the steering wheel and thus provides the mechanical feedback to the operator. The controller is designed to emulate the traditional mechanical resistance.

Because the steering wheel has a large range of movement from the neutral position to  $\pm 570^\circ$ , Different control laws for the DC motor for different ranges of the angle are designed. The control switches according to the angle and angular velocity. The flow chart in Figure 4.5 shows the switching law.

Driving an agriculture machine is the same as driving a car and most of the time, it is desirable that the steering wheel has the tendency to turn to the neutral position with a proper speed after the vehicle turn has been completed. But the

operator may like to keep the steering wheel to be fixed at a certain angle when making a big circular turn in which case the steering wheel often goes through a big range. With these requirements, the tactile controllers of the switching control are designed as described below.

When the angle is small such that  $abs(\theta) \leq \theta_{lin} = 5^\circ$ , the PI control is used to provide a resistant torque proportional to the angle and to the angular velocity. The element that is proportional to the angular velocity provides damping which reduces oscillations near the neutral position. The output voltage of the controller is

$$C_1 = -K_{p\_lin} \cdot \omega - K_{i\_lin} \cdot \theta, \quad (4.9)$$

where  $\omega$  is the angular velocity of the steering wheel and  $\theta$  is the angle of the steering wheel. This notation applies to all the following PI controllers.  $K_{p\_lin}$  and  $K_{i\_lin}$  are the proportional gain and integral gain of the PI controller respectively.

When the angular position is in the range  $\theta_{lin} = 5 \leq abs(\theta) \leq \theta_{prelock} = 540$ , the control switches to the second branch which is the main operating range. In this branch, either the second or the third control is active depends on whether the directions of the angle and angular velocity are the same or the opposite. If it is desired that the steering wheel should be turned back to zero position, then the directions of the position and angular velocity can be made different by pulling the steering wheel toward the zero position. In this case, the second controller is active. The steering wheel is turned back to zero by a torque which has a constant part given by  $-K_{i\_prelock} \cdot sign(\theta)$ . Because of the large range of the angle, the resistance torque would vary in a large range if the torque were proportional to the angle, thus would not provide a smooth driving feel through the whole range. Furthermore, the damping torque proportional to the angular velocity are needed to regulate the steering wheel speed. Thus, the output voltage of the controller is:

$$C_2 = -K_{p\_prelock} \cdot \omega - K_{i\_prelock} \cdot sign(\theta), \quad (4.10)$$

where  $K_{p\_prelock}$  is the proportional gain of the PI controller and  $K_{i\_prelock}$  is the integral gain of the PI controller. The gain  $K_{i\_prelock}$  is designed by choosing  $K_{i\_prelock} = K_{i\_lin} \cdot \theta_{lin}$  so that the resistant torque is continuous when the control is switched between the first and second branches.

When the angle and angular velocity of the steering wheel are of the same sign, the third control becomes active. In this case, only the damping torque is provided. With the friction of the steering column, the steering wheel can be kept still at a desired position. The control law is designed as:

$$C_3 = -K_{p\_prelock} \cdot \omega. \quad (4.11)$$

The second controller and the third controller can be combined as

$$C_{23} = -K_{p\_prelock} \cdot \omega - \frac{1}{2}K_{i\_prelock} * (\text{sign}(\theta) - \text{sign}(\omega)). \quad (4.12)$$

So in the main operating range, when the steering wheel is not turned further ahead, it can either be kept at that position or turned back to the zero position automatically depending on the operator's desire.

When the angle is in the range  $\theta_{prelock} = 540 \leq \text{abs}(\theta) \leq \theta_{lock} = 570$ , the fourth controller is active. In this range, the controller produces a sine wave output voltage to alert the operator that the turning limit is reached. The steering wheel will oscillate hardly like driving on rocky roads. This warning can be eliminated by pulling the steering wheel back to  $\text{abs}(\theta) \leq 540$ . The control law of the fourth controller is

$$C_4 = -K_{i\_lock} \cdot (1 + \epsilon \sin(10t)), \quad (4.13)$$

where  $0 < \epsilon < 1$ ,  $t$  is time and  $K_{i\_lock}$  is the integral gain of the PI controller.

If the operator ignores the warning and turns the steering wheel further, the resistance is set to be very big and the operator will feel very hard to turn the

steering wheel. The resistant is still a constant torque opposite to the angle direction plus a damping term.

$$C_5 = -K_{p\_postlock} \cdot \omega - K_{i\_postlock} \cdot \text{sign}(\theta). \quad (4.14)$$

In this research project, the encoder used to measure the angle and angular velocity has a zero position index. The zero position index can be used to rectify position fault due to miss counting, which has been simulated in laboratory. When rectification angle occurs at the zero position, the instantaneous angular velocity of the steering wheel is not measured correctly because there is a jump of the angle.

#### 4.5 Stability Analysis

For the last four branches of the control, the steering angle will go to its previous branch if there is no external torque disturbance. For example, when there is no external torque, the steering wheel angle will go from branch 5 to branch 4, then to branch 3, and so on, automatically. Finally, it settles down in the first branch. So the stability of the switching control system is achieved if the first branch is stable.

From the last chapter, we know that the discrete transfer function for the steering wheel including the angular sensor and the DC geared motor is

$$\frac{\Omega(z)}{V(z)} = \frac{0.0248}{1 - 0.15341z^{-1} - 0.7907z^{-2}}. \quad (4.15)$$

where  $\Omega(z)$  is the z-transform of the angular velocity and  $V(z)$  is the z-transform of the control voltage. This discrete transfer function is transformed into continuous form by using the conversion method of zero order hold. The zero order hold conversion increases the model order for systems with real negative poles in the  $z$  plane since a real negative pole is mapped to a pair of conjugate complex poles in the  $s$  plane. To ensure that all complex poles of the continuous model come in conjugate pairs, the Matlab command `d2c` replaces negative real poles with a pair of

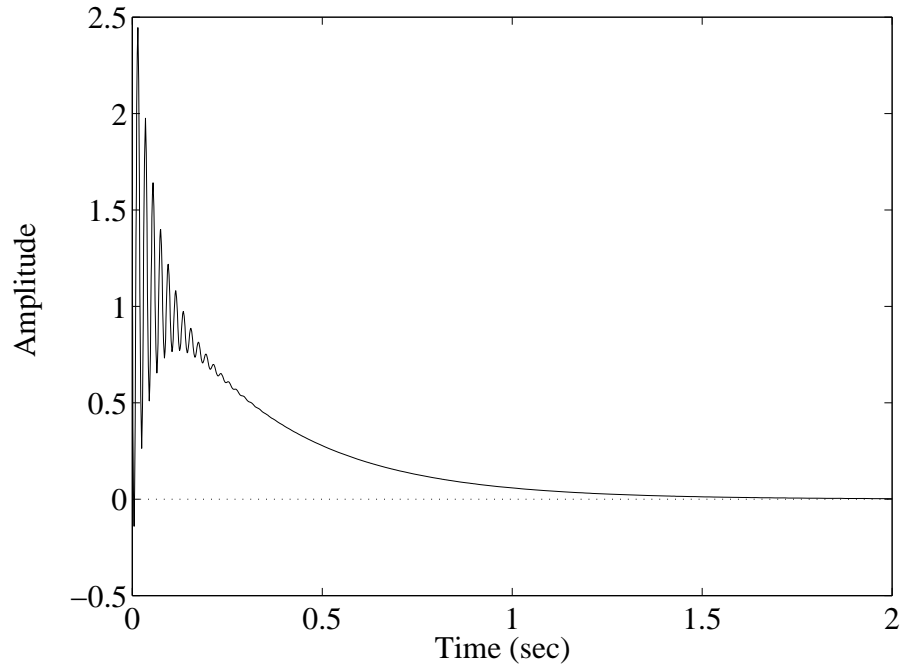


**Figure 4.6:** The impulse response shows that the plant is stable.

complex conjugate poles near these negative real poles. The conversion then yields a continuous model with higher order and the system transfer function becomes:

$$G(s) = \frac{\Omega(s)}{V(s)} = \frac{0.0248s^3 + 2.309s^2 + 2010s + 137500}{s^3 + 43.84s^2 + 99240s + 309900}. \quad (4.16)$$

The poles of the plant transfer function are  $-20.36+314.16i$ ,  $-20.36-314.16i$ , and  $-3.13$ , which are all in the left half of the  $s$  domain. The impulse response of the plant is shown in Figure 4.6. The step response of the plant is shown in Figure 4.7, which indicates the slow response of the system. Its rise time is around 0.7 sec. Since there is no oscillation in the step response, the plant has a large damping.

The control law of the first branch can be expressed as:

$$D(s) = K_{p\_lin} + \frac{K_{i\_lin}}{s}. \quad (4.17)$$

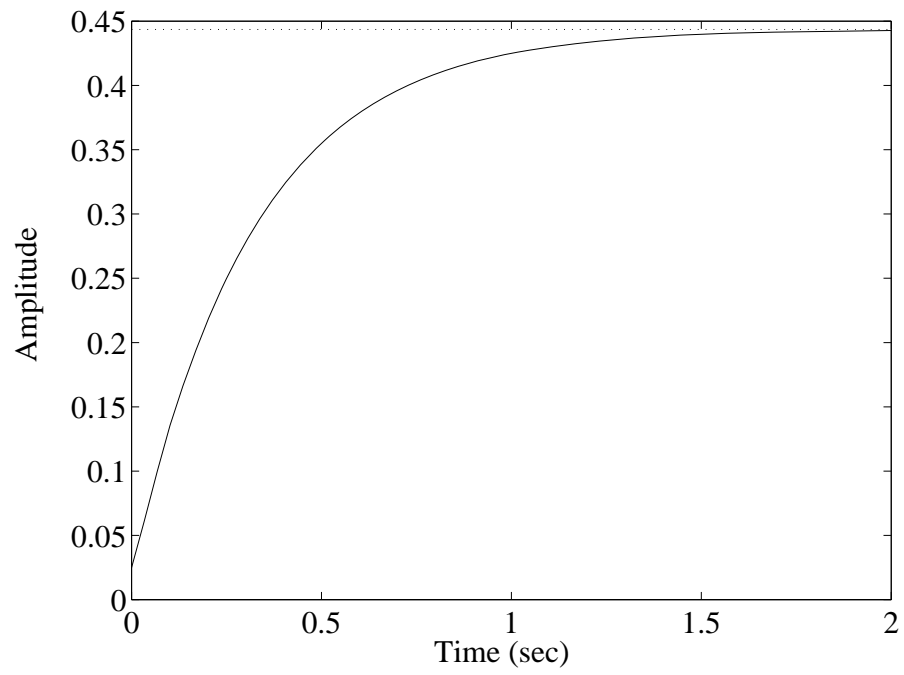


**Figure 4.7:** The step response of the plant shows that it is a slow system. The rise time is around 0.7 second.

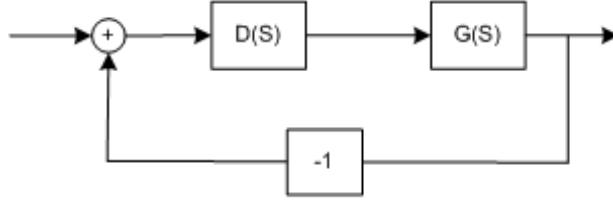


**Figure 4.8:** Diagram of closed transfer function.

The closed transfer function is

$$H(s) = \frac{b(s)}{a(s)}, \quad (4.18)$$

where

$$\begin{aligned} b(s) = & 0.0248K_{p\_lin}s^4 + (2.309K_{p\_lin} + 0.0248K_{i\_lin})s^3 + (2010K_{p\_lin} + 2.309K_{i\_lin})s^2 \\ & + (137500K_{p\_lin} + 2010K_{i\_lin})s + 137500K_{i\_lin}, \end{aligned} \quad (4.19)$$

and

$$\begin{aligned} a(s) = & (0.0248K_{p\_lin} + 1)s^4 + (2.309K_{p\_lin} + 0.0248K_{i\_lin} + 43.84)s^3 \\ & + (2010K_{p\_lin} + 2.309K_{i\_lin} + 99240)s^2 + (137500K_{p\_lin} + 2010K_{i\_lin} + 309900)s \\ & + 137500K_{i\_lin}. \end{aligned} \quad (4.20)$$

$a(s)$  gives the system characteristic function. We use Routh's stability criterion to determine the range of control parameters  $K_{p\_lin}$  and  $K_{d\_lin}$ . The necessary condition for the stability is that all the coefficients of the characteristic polynomial

be positive. The following conditions have to be satisfied:

$$\begin{aligned}
P(1) &= 0.0248K_{p\_lin} + 1 > 0, \\
P(2) &= 2.309K_{p\_lin} + 0.0248K_{i\_lin} + 43.84 > 0, \\
P(3) &= 2010K_{p\_lin} + 2.309K_{i\_lin} + 99240 > 0, \\
P(4) &= 137500K_{p\_lin} + 2010K_{i\_lin} + 309900 > 0, \\
P(5) &= 137500K_{i\_lin} > 0.
\end{aligned} \tag{4.21}$$

which is equivalent to

$$\begin{aligned}
K_{p\_lin} &> -40.32, \\
K_{p\_lin} &> -0.011K_{i\_lin} - 18.99, \\
K_{p\_lin} &> -0.001K_{i\_lin} - 49.37, \\
K_{p\_lin} &> -0.015K_{i\_lin} - 2.25, \\
K_{i\_lin} &> 0.
\end{aligned} \tag{4.22}$$

From Figure 4.9, it can be derived that the effective constraints are,  $K_{p\_lin} > -0.015K_{i\_lin} - 2.25$ , for  $0 < K_{i\_lin} < 2538$  and  $K_{p\_lin} > -40.32$  for  $K_{i\_lin} > 2538$ .

According to Routh and Hurwitz stability criterion, the necessary and sufficient condition for the system stability is that all elements in the first column of the Routh array expressed by Equation (4.23) are positive.

$$\begin{array}{cccc}
s^4 & P(1) & P(3) & P(5) \\
s^3 & P(2) & P(4) & 0 \\
s^2 & P(6) & P(7) & 0 \\
s^1 & P(8) & 0 & 0 \\
s^0 & P(9) & 0 & 0
\end{array} , \tag{4.23}$$

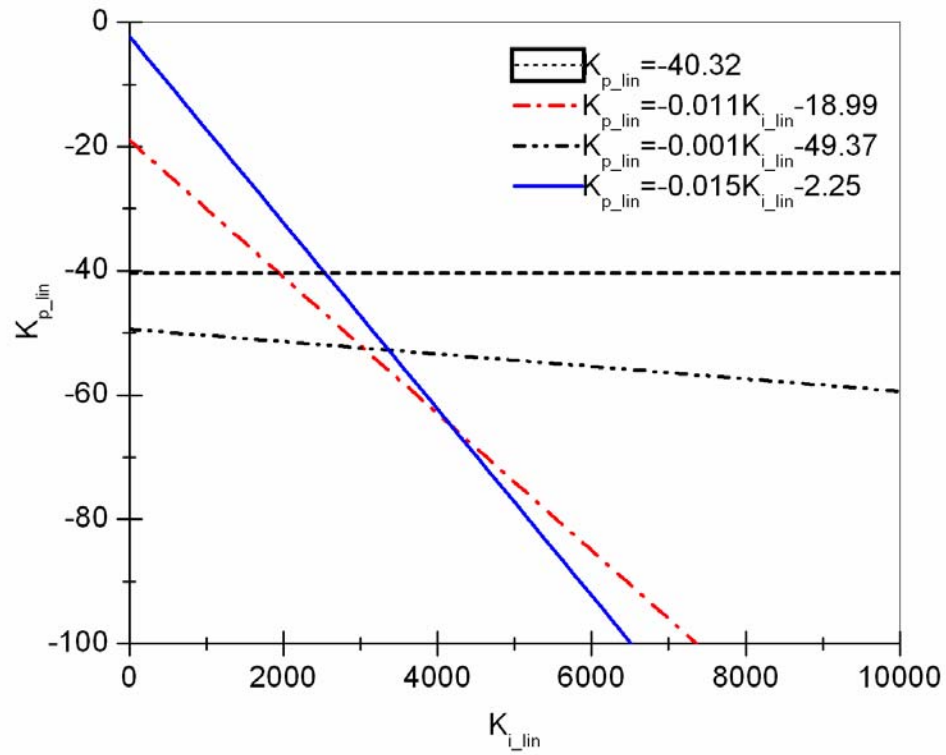


**Figure 4.9:** The necessary condition of Routh's stability test is that all the parameters in closed system transfer function is greater than zero. That is the control parameter  $K_p$  and  $K_i$  should be above all the lines in the above diagram.

where  $P(1) - P(5)$  were defined in equation (4.21).  $P(6) - P(9)$  will be given below. The system is stable if  $P(1), P(2), P(6), P(8), P(9)$  are all positive.  $P(6)$  is expressed as Equation (4.24).

$$P(6) = -\frac{\det \begin{bmatrix} P(1) & P(3) \\ P(2) & P(4) \end{bmatrix}}{P(2)} \quad (4.24)$$

Because  $P(2)$  is greater than zero when the necessary condition is satisfied, the numerator of  $P(6)$  needs to be greater than zero for the system to be stable according to Routh's stability criterion. Equation (4.25) is the numerator of  $P(6)$ .

$$\begin{aligned} & -\det \begin{bmatrix} P(1) & P(3) \\ P(2) & P(4) \end{bmatrix} \quad (4.25) \\ & = 1231.09K_{p\_lin}^2 + 5.33K_{p\_lin} * K_{i\_lin} + 0.057K_{i\_lin}^2 \\ & + 172078.04K_{p\_lin} + 552.38K_{i\_lin} + 4040781.6 > 0 \end{aligned}$$

Under the necessary condition  $K_{i\_lin} > 0$ , if we assume  $K_{i\_lin}$  is constant, Equation (4.25) is a increasing function of  $K_{p\_lin}$ . So equation (4.25) achieves its minimum value when  $K_{p\_lin} = -0.015K_{i\_lin} - 2.25$ . Equation (4.25) is guaranteed to be positive for  $0 < K_{i\_lin} < 1856.34$ . It is easy to show that  $P(6)$  is positive for the controller, because from the experiment,  $K_{i\_lin}$  is a small value compared to 1856.34.  $P(7)$  equals to  $P(5)$  and is positive as shown in Equation (4.26):

$$P(7) = -\frac{\det \begin{bmatrix} P(1) & P(5) \\ P(2) & 0 \end{bmatrix}}{P(2)} = P(5) > 0. \quad (4.26)$$

$P(8)$  is calculated by Equation (4.27) as:

$$P(8) = -\frac{\det \begin{bmatrix} P(2) & P(4) \\ P(6) & P(7) \end{bmatrix}}{P(6)} > 0. \quad (4.27)$$

Because  $P(6)$  is positive according to the above statements, the numerator of  $P(8)$  needs to be positive for the system to be stable according to Routh's stability criterion. Equation (4.28) which is the numerator of  $P(8)$  is shown below:

$$\begin{aligned}
& - \det \begin{bmatrix} P(2) & P(4) \\ P(6) & P(7) \end{bmatrix} \\
& = P(4)P(6) - P(2)P(7) \\
& = P(3)P(4) - P(1)P(4)P(4)/P(2) - P(2)P(5) \\
& = (2010kp + 2.309ki + 99240)(137500kp + 2010ki + 309900) - 137500(2.309kp \\
& + 0.0248ki + 43.84)ki - \frac{(0.0248kp + 1)(137500kp + 2010ki + 309900)^2}{2.309kp + 0.0248ki + 43.84} > 0.
\end{aligned} \tag{4.28}$$

Equation (4.28) is greater than zero when  $K_{p\_lin} \geq 0$  and  $K_{i\_lin} \geq 0$ . The optimization tool box of Maple is used to find the minimum value of Equation (4.28) with the command  $LPSolve(p8num, \{K_{p\_lin} \geq -0.015 * K_{i\_lin} - 2.25, K_{i\_lin} \geq 0\}, assume = nonnegative)$ . The minimum value of Equation (4.28) is  $0.2856 * 10^{11}$  when  $K_{p\_lin} = 0$  and  $K_{i\_lin} = 0$ . Through trial and error we can guarantee that  $P(8)$  is greater than zero when  $K_{p\_lin} \geq -2.25$  and  $K_{i\_lin} \geq 0$ .  $P(9)$  equals to  $P(5)$  and is positive as shown in Equation (4.29):

$$P(9) = - \frac{\det \begin{bmatrix} P(6) & P(7) \\ P(8) & 0 \end{bmatrix}}{P(8)} = P(7) = P(5) > 0. \tag{4.29}$$

So, according to Routh's stability criterion, the system is stable when  $K_{p\_lin} \geq -2.25$  and  $0 \leq K_{i\_lin} \leq 1856.34$ .

## 4.6 Simulations

The tactile feedback control system is a human-machine interface system where the participation of human being into the system brings in a lot of uncertain factors. It is required that the system should be flexible and adaptive to these

uncertainties. According to the above arguments, we know that the tactile feedback system is stable under a great range of control parameters. The controller gains are left for the user to decide depending on their requirements. The following table provides a guidance for selecting the control gains.

**Table 4.1:** Effects of PI controller parameters on the closed-loop system response. This can be a guidance of PI tuning for Tactile feedback control system.

C.L RES	RISE TIME	OVER SHOOT	SETTLING TIME	S-S ERROR
Ki	Decrease	Increase	Small Change	Decrease
Kp	Small Change	Decrease	Decrease	Small Change

Simulations are provided to show that the system can follow a unit step signal well with various control gains. The following are the responses of the control systems at different control gains. The analysis of their performance are also presented.

(1) when  $K_{p\_lin} = -1$ ,  $K_{i\_lin} = 10$ . Both rise time and over shoot are big, but the steady state error is zero.

(2) when  $K_{p\_lin} = -1$ ,  $K_{i\_lin} = 50$ . Here proportional gain  $K_{p\_lin}$  is unchanged and integral gain  $K_{i\_lin}$  is increased. Rise time is decreased and over shoot is increased and the steady state error is zero.

(3) when  $K_{p\_lin} = 10$ ,  $K_{i\_lin} = 10$ . Here proportional gain  $K_{p\_lin}$  is increased to a positive value and integral gain  $K_{i\_lin}$  decreases to 10. Both rise time and over shoot are decreased to a small value and the steady state error is zero. This is a fairly good control system.

(4) when  $K_{p\_lin} = 50$ ,  $K_{i\_lin} = 200$ . Both proportional gain  $K_{p\_lin}$  and integral gain  $K_{i\_lin}$  are increased dramatically. The output signal follows the input signal perfectly.

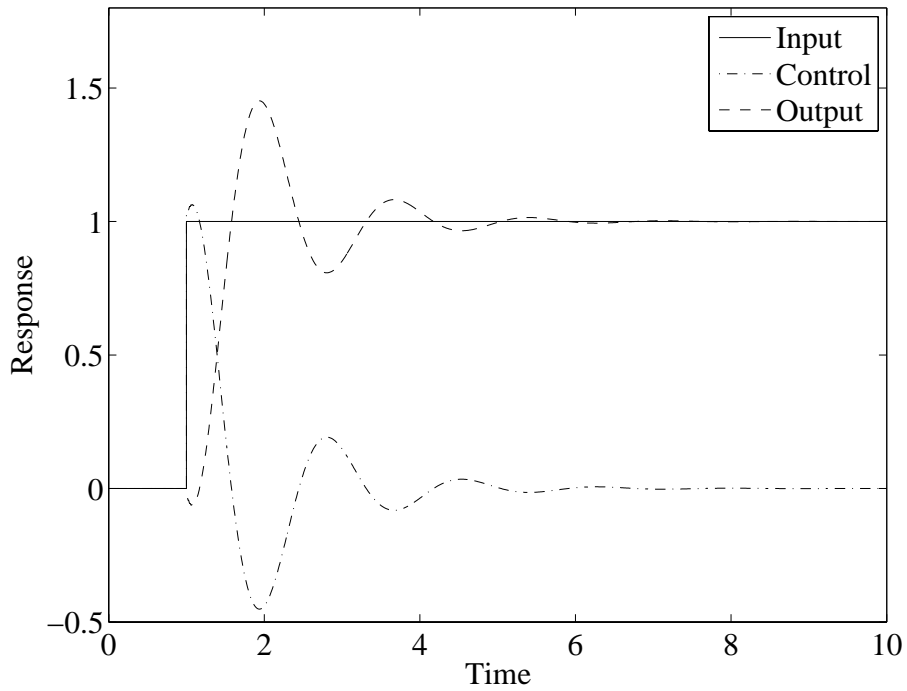


**Figure 4.10:** Step response of the PI controller with  $K_{p\_lin} = -1$ ,  $K_{i\_lin} = 10$ . The solid line represents the step input signal. The dash-dot line is the control signal. The dashed line is the output response. The rising time and over shoot are all big. Steady state error is zero.

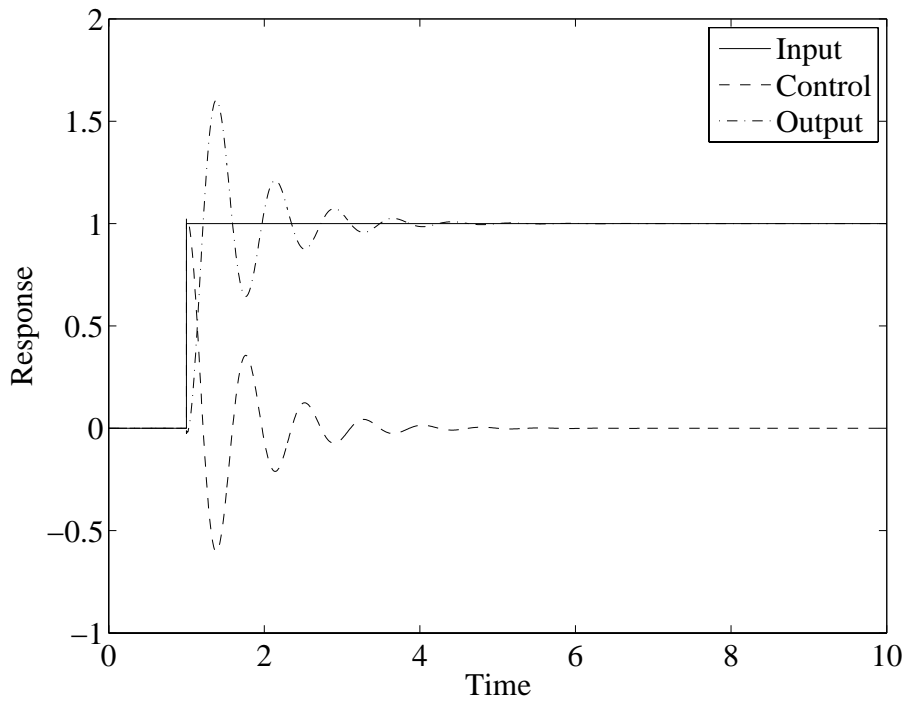


**Figure 4.11:** Step response of the PI controller with  $K_{p\_lin} = -1$ ,  $K_{i\_lin} = 50$ . The solid line represents the step input signal. The dashed line is the control signal. The dash-dot line is the output response. Rising time decreases and over shoot gets bigger. Steady state error is zero.

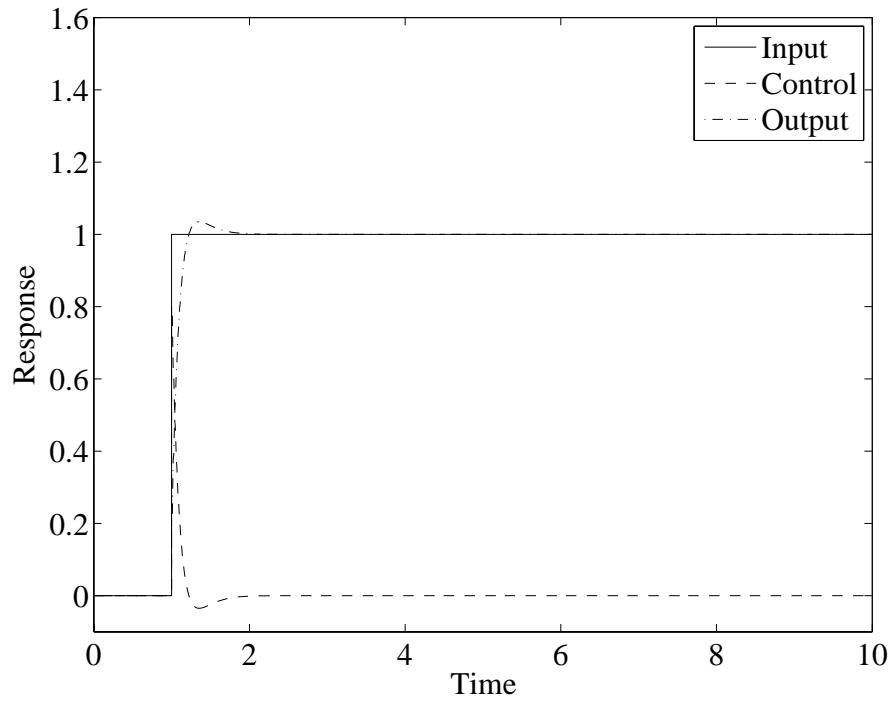


**Figure 4.12:** Step response of the PI controller with  $K_{p\_lin} = 10$ ,  $K_{i\_lin} = 10$ . The solid line represents the step input signal. The dashed line is the control signal. The dash-dot line is the output response. Both rising time and over shoot are decreased to a small value. Steady state error is zero.

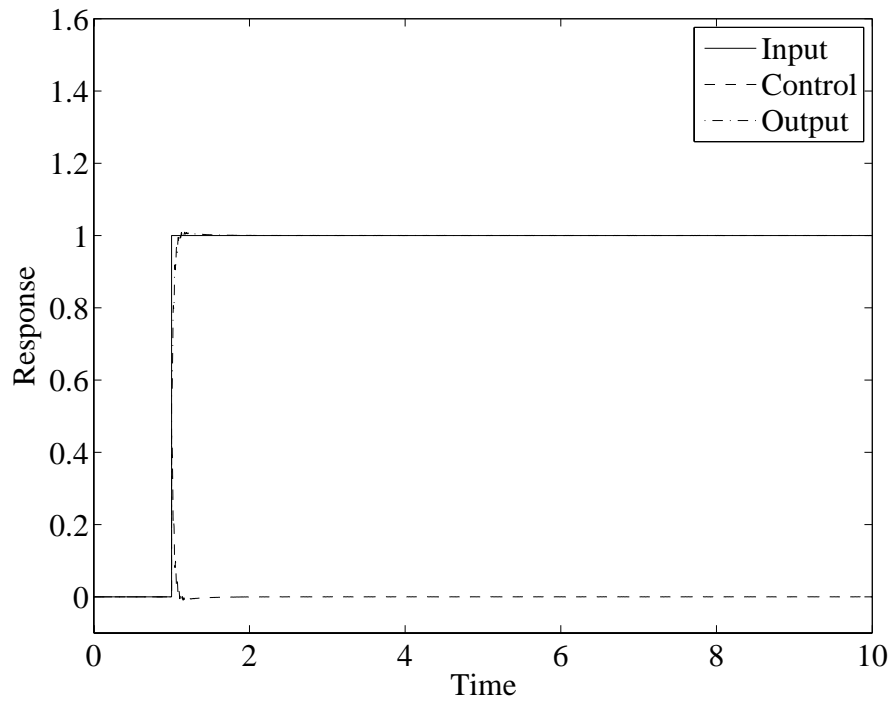


**Figure 4.13:** Step response of the PI controller with  $K_{p\_lin} = 50$ ,  $K_{i\_lin} = 200$ . The solid line represents the step input signal. The dashed line is the control signal. The dash-dot line is the output response. The output signal follows the input signal perfectly.

Table 4.2 shows the control gains used in the laboratory for the hardware in loop simulation. This experiment system is different from the one discussed above which is the real system used on steer-by-wire agriculture machines.

**Table 4.2:** Control parameters used for hardware-in-loop simulation.

Param	Linear	Pre-Lock	Lock	Post-Lock
$K_p$	0.005	0.005	–	8
$K_i$	0.8	2	10	0.02

## Chapter 5

### SUMMARY

In this section a summary of the thesis is briefly discussed. Steer-by-wire agriculture machines have the advantages of simpler assembly structure, higher machine design flexibility and lower production costs compared to conventional agriculture machines. The implementation of steer-by-wire system includes two tasks. The first task is the control of vehicle propulsion and the second task is the tactile feedback control. The development in both tasks of steer-by-wire systems have been contributed by different research groups. Current research is focused on the tactile feedback system that is applicable to heavy off-road steer-by-wire vehicles without using torque sensors, whose main function is to emulate the mechanical resistance in conventional vehicles.

To achieve tactile feedback control, the conventional steering column has been modified by mounting a quadrature encoder and a DC geared motor to the bottom of the steering shaft. The two output channels of the quadrature encoder are fed to the vehicle control module which is called XCM. Then the angle and angular velocity and their directions of the steering wheel have been estimated, which are the input signals of the tactile feedback controller. The steer-by-wire control algorithm and other vehicle functions are implemented through XCMs. The DC geared motor is regulated by the tactile feedback controller to produce the emulated resistance during the operation of the vehicle. To achieve reversible rotation of the DC geared motor, an H-bridge circuit is integrated in the XCM control module to provided both positive and negative power supply to the DC geared motor.

The tactile feedback system model has been identified. Experiments have been designed and implemented to collect input and output signals of the tactile feedback system. The signals are analyzed by Fast Fourier Transform and the system Bode plot is plotted, which implies the system has a low order. FIR models and IIR models of different orders are tested for the best model structure and a second order IIR filter is chosen to model the system transfer function. The convergence of model parameter vector is verified. The model simulated output and the true system output are coincident at low frequencies.

The designed tactile feedback control system consists two loops, the outer loop is the tactile feedback controller and the inner loop is an electrical current control. For the outer loop, the tactile feedback controller regulates the DC geared motor to produce tactile feedback torque. Because of the big range of steering angle, a single control law will not provide accurate regulations in the whole driving process. Thus the tactile feedback controller is designed as a switching controller with five branches. According to the angle and angular velocity of the steering column, only one of the five branches will be active at the same time. The inner loop electrical current controller whose stability has been verified regulates the variation of DC motor current due to environmental change. Because the tactile feedback control system is a human-machine interface system, it is desired that the user have the flexibility to choose tactile feedback control gains. The stability of the tactile feedback controller is guaranteed for a huge range of the control gains. Examples of control gains and the system performance under these gains have been demonstrated by Simulation.

## BIBLIOGRAPHY

- [1] N. Bajcinca, R. Cortesao, M. Hauschild, J. Bals, and G. Hirzinger. Haptic control for steer-by-wire systems. In *Proceedings of IEEE International Conference on Intelligent Robots and Systems*, volume 2, pages 2004–2009, Las Vegas, NV, United States, 2003.
- [2] S. Bolognani, M. Tomasini, and M. Zigliotto. Control design of a steer-by-wire system with high performance pm motor drives. In *Proceedings of IEEE Annual Power Electronics Specialists Conference*, volume 2005, pages 1839–1844, 2005.
- [3] X. Chen, X. Chen, and K. Li. Robust control of electric power-assisted steering system. In *Proceedings of IEEE Vehicle Power and Propulsion Conference*, volume 2005, pages 97–102, Chicago, IL, United States, 2005.
- [4] R. Cortesao and N. Bajcinca. Model-matching control for steer-by-wire vehicles with under-actuated structure. In *Proceedings of IEEE/RSJ International Conference on Intelligent Robots and Systems*, volume 2, pages 1148–1153, Sendai, Japan, 2004.
- [5] C. A. Foster. *Intelligent Control Study of Driver-by-wire Agriculture Vehicles*. Dissertation, University of Delaware, Newark, 2005.
- [6] C. A. Foster, R. P. Strosser, J. Peters, and J.-Q. Sun. Automatic velocity control of a self-propelled windrower. *Computers and Electronics in Agriculture*, 47(1):41–58, 2005.
- [7] D. Gualino and I.-J. Adoukpe. Force-feedback system design for the steer-by-wire: optimisation and performance evaluation. In *Proceedings of IEEE Intelligent Transportation Systems Conference*, Toronto, Canada, 2006.
- [8] S. Haggag, D. Alstrom, S. Cetinkunt, and A. Egelja. Modeling, control, and validation of an electro-hydraulic steer-by-wire system for articulated vehicle applications. *IEEE/ASME Transactions on Mechatronics*, 10(6):688–692, 2005.
- [9] J. Melli Huber, B. Weinberg, A. Fisch, J. Nikitzuk, C. Mavroidis, and C. Wampler. Electro-rheological fluidic actuators for haptic vehicular instrument controls. In *Proceedings of the 11th Symposium on Haptic Interfaces for Virtual Environment and Teleoperator Systems*, 2003.

- [10] S.-H. Jang, T.-J. Park, and C.-S. Han. A control of vehicle using steer-by-wire system with hardware-in-the-loop-simulation system. In *Proceedings of Advanced Intelligent Mechatronics*, 2003.
- [11] Y. Lee and W.-S. Lee. Hardware-in-the-loop simulation for electro-mechanical brake. In *Proceedings of SICE-ICASE International Joint Conference*, pages 1513–1516, Busan, South Korea, 2006.
- [12] R. Nossal and R. Lang. Model-based system development. *IEEE Micro*, 22(4):56–63, 2002.
- [13] M. Parmar and J. Y. Hung. A sensorless optimal control system for an automotive electric power assist steering system. *IEEE Transactions on Industrial Electronics*, 51(2):290–298, 2004.
- [14] J. Ryu and H. Kim. Virtual environment for developing electronic power steering and steer-by-wire systems. In *Proceedings of IEEE International Conference on Intelligent Robots and Systems*, volume 3, pages 1374–1379, Kyongju, South Korea, 1999.
- [15] P. Setlur, J. Wagner, D. Dawson, and L. Powers. A hardware-in-the-loop and virtual reality test environment for steer-by-wire system evaluations. In *Proceedings of the American Control Conference*, volume 3, pages 2584–2589, Denver, CO, United States, 2003.
- [16] P. Yih and J. C. Gerdes. Modification of vehicle handling characteristics via steer-by-wire. *IEEE Transactions on Control Systems Technology*, 13(6):965–976, 2005.
- [17] H. Zang and M. Liu. Fuzzy neural network PID control for electric power steering system. In *Proceedings of the IEEE International Conference on Automation and Logistics*, pages 643–648, Jinan, China, 2007.